Aalto University
School of Engineering

Aalto University
School of Engineering
Civil Engineering Department

D1.4. Non-Destructive Testing Methods for Corrosion Assessment of Rock Bolts: State-of-the-Art Survey

PERCO2 2025 / WP1 – Durability testing of existing concrete specimens

Fahim Al-Neshawy and Abobaker Ba Ragaa

Olkiluoto's research area housed 350m underground. Photo: Peter Guenze
https://scanclimber.com/finnish-nuclear-waste-terminal-placement/

Aalto University School of Engineering, Department of Civil Engineering
PL 12100, FI-00076 AALTO
http://civileng.aalto.fi

Table of Contents

1 Introduction

This research report focuses on the latest advancements in non-destructive testing (NDT) methods for detecting corrosion in rock bolts. In the spring of 1993, ten test rock bolts were installed in the research tunnel of the Olkiluoto LILW cave to assess the corrosion rate of rock reinforcement bolts under the LILW cave conditions. The rock bolts are made of the same material as the high-strength steel bolts used in the roof of the LILW cave crane hall, specifically A500H hot-dip galvanized and passivated, with a diameter of 25 mm and a length of 2400 mm (2.4 m). The bolts were grouted using standard Portland cement mortar, as was done in the crane hall, with approximately 100 mm of the bolt ends exposed. The cement mortar contained sand with a grain size of 0 to 2 mm in a mix ratio of 1:1, and the water-cement ratio was 0.5.

The bolt holes were drilled with compressed air to a diameter of 38 - 40 millimetres, which is smaller than the hole diameter used in the crane hall ceiling (45 mm). This allows space around the test bolts for a thinner layer of joint mortar, leading to earlier failure of the chemical protection. Therefore, it was not deemed necessary to leave un-mortared zones around the bolts, although the initial intention was to do so to simulate cracks formed in the cement mortars.

Detecting corrosion in rock bolts is crucial for maintaining structural integrity, especially in underground environments. Non-destructive testing (NDT) methods are essential for assessing the condition of installed rock bolts, as visual inspection alone can be misleading [1]. The objective of this state-of-the-art report is presenting a literature review about the most reliable NDT methods for detecting the corrosion of rock bolts in the Low- and Intermediate Level Waste (LILW) repository structures. The review includes investigation of the different anchor bolt types used in the Low- and Intermediate Level Waste (LILW) repository structures, the corrosion mechanisms of the anchor bolt and the potential NDT methos for detection of the anchor bolt corrosion.

1.1 Rock bolts vs. rock anchors

In geotechnical engineering, rock bolts and rock anchors are critical tools for stabilizing rock masses and structures. Though often confused, they serve distinct purposes and operate under different principles. Both rock bolts and rock anchors the key terms essential for ensuring the safety and durability of structures [2].

Rock bolts serve as reinforcement components in geotechnical engineering, intended to stabilize rock formations within tunnels, mines, slopes, and excavations. They work by binding loose or unstable rock layers into a unified, solid structure, thereby improving stability and reducing the likelihood of collapse.

Rock anchors are a structural reinforcement system designed to transfer loads from a structure to stable bedrock, ensuring stability and resistance to forces such as uplift, overturning, and lateral movement. Commonly used in geotechnical and civil engineering, rock anchors enhance the structural integrity of infrastructure projects, including dams, bridges, retaining walls, and high-rise buildings.

While both rock bolts and rock anchors stabilize geological and structural systems, their functions differ significantly. Rock bolts provide internal reinforcement by integrating fractured rock, whereas rock anchors transfer structural loads to deeper, stable bedrock. Understanding these differences is essential for selecting the appropriate solution, ensuring structural stability and long-term performance [2].

Table 1. Key differences and applications of rock anchors and rock bolts [2].

Feature	Rock Bolt	Rock Anchor
Primary Role	Reinforced Rock Mass	Anchor Structures to bedrock
Load Type	Shear/Tension within rock	Tensile (structural loads)
Length	1-10 meters	10-50 meters
Installation	Grouted or mechanical, often un-tensioned	Grouted + tensioned
Common Use Cases	Tunnels, mines	Dams, bridges, skyscrapers

1.2 Cement grouted rock bolts

Cement grouted rock bolts, shown in Figure 1, make use of cement to bond the bolts to the walls of drilled boreholes. The cement grouted bolts have a longer curing time and cannot be applied in boreholes with flow of water. The presence of groundwater in a hole prevents the curing of the cement.

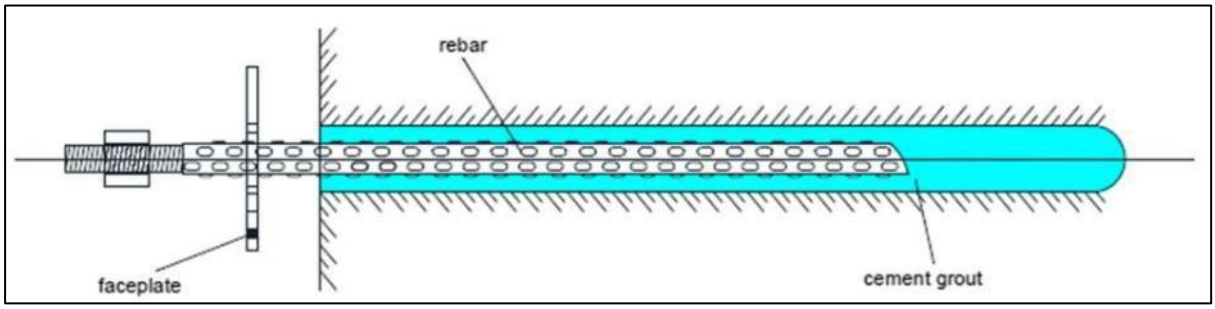

Figure 1. Image of cement grouted bolt [3].

During installation of the cement grouted bolts, as presented in Figure 2, the following steps should be performed [4]:

1) Site inspection and safety preparation

   A complete site inspection for rock conditions must be performed before starting rock bolt installation. Evaluate areas prone to weakness and determine bolt placement locations.

2) Drilling the borehole

A rock drill operator should make boreholes at each marked position. The borehole needs to have dimensions that correspond exactly to the measurements of the rock bolts that will be inserted. A clean hole free of loose debris must exist because such material could reduce bolt anchorage performance.

3) Grouting of the borehole

   Inject cement grout into the hole before inserting the bolt.

4) Inserting the rock bolt

   Carefully insert the rock bolt into the grouted drilled hole. However, after installation, it takes hours or days to be properly cured or before gaining its full strength.

5) Securing and tensioning the bolt

   After insertion tighten the bolt with a torque wrench or hydraulic tensioner to achieve proper security. Appropriate bolt tensioning improves both the load-carrying ability and long-term stability of the bolt.

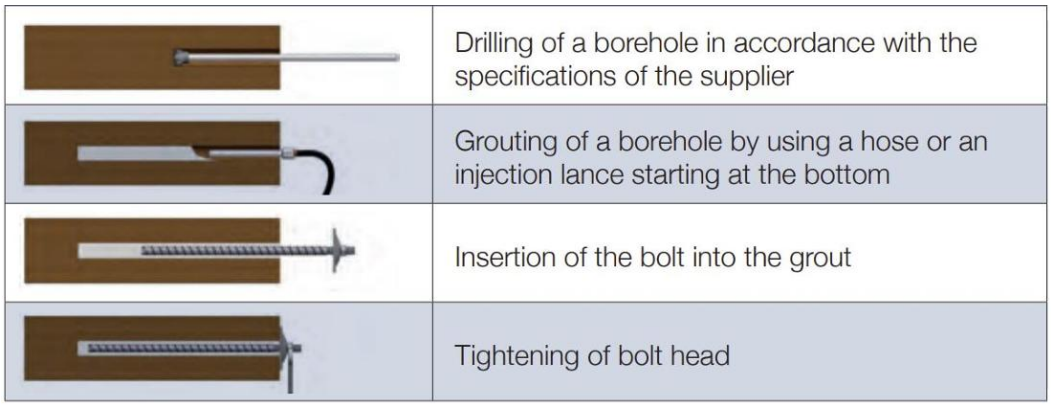

Figure 2. Installation procedure of the cement grouted bolts,

The cement grouted rock bolts have the capacity to support the dead weight of key blocks up to 10 tons and perform better as reinforcement tools in weak strata. The disadvantage is the issue of cement shrinkage, which reduces the bonding strength between the rock and wall of the borehole [5].

2 Corrosion mechanism of rock bolts

Corrosion is a physical alteration of a material from electrochemical reaction with its environment that often results in reduction of the mechanical properties of that material. Rock bolts are particularly susceptible to corrosion as they can be exposed in their working environment to ground water. Corrosion increases markedly in sulphide ore bodies due to acid runoff. Table blow shows different types of corrosion that a rock bolt is likely to undergo when used for Low- and Intermediate Level Waste (LILW) repository structures reinforcement [6].

2.1 Aggressive environmental conditions

The identify key environmental parameters affecting the corrosion of rock bolts coincide in the following water properties as relevant [7], [8], [9]:

1) **Ground water pH levels**: Regarding the pH in groundwater, a pH of water below four is an important water property to promote corrosion. If the rock contains the mineral pyrite (FeS_2), which under the presence of oxygen and water, it oxidizes creating sulfuric acid. The pH in ground water Loviisa is around 7,6 and the sulfate ion concentration is 470 to 590 mg/l, while the pH in ground water Olkiluoto is around 8,9 and the sulfate ion concentration is 45 mg/l. The acidity or alkalinity of the environment can alter the rate of metal dissolution. Low pH conditions (acidic environments) are typically more aggressive, promoting faster corrosion than neutral or basic conditions. Testing the pH of the surrounding environment can provide valuable information for predicting corrosion behaviour.
2) **Salinity** (according to either the Cl^- ions and $SO4^{2-}$ content, electrical resistivity, or total dissolved solids in groundwater): A high chloride content has been identified in the groundwater of Loviisa. The results of water samples from different tunnel locations in Loviisa indicate that the chloride concentration range is between 4000 mg/l and 5250 mg/l. With this concentration level, tunnels fall into the highest salinity level in all the rankings mentioned. The chloride ion in Olkiluoto is between 17 and 18 mg/l, which falls in low salinity level. Chloride ions, commonly found in groundwater, can penetrate protective layers on metals, leading to localized forms of corrosion such as pitting.
3) **Concentration of dissolved oxygen**: The occurrence of high concentrations of dissolved oxygen is expected in Nordic underground structures due to a general low groundwater temperature (< 7 °C) [16]. Although dissolved oxygen content in groundwater generally decreases with depth, high concentrations can be found at deep depths if the aquifer is permeable and connected to a brook. Thus, Nordic underground structures with permeable rock and low overburden are susceptible to have groundwater with high concentrations of dissolved oxygen. Oxygen availability plays a crucial role in electrochemical reactions leading to corrosion. The concentration of oxygen in the environment can dictate the rate of cathodic reduction processes, affecting overall corrosion rates. For example, in submerged environments where oxygen levels are low, corrosion may proceed at a different rate compared to aerated conditions.

Galvanic corrosion is more severe in high humidity and saline environments, where these factors act as electrolytes, intensifying the electrochemical reaction between metals.

2.2 Electrochemical corrosion principle

The corrosion process is an important reference for identifying the corrosion of anchor bolts in rock masses. The corrosion forms of anchor bolts include uniform corrosion, pitting corrosion, and stress corrosion, among others.

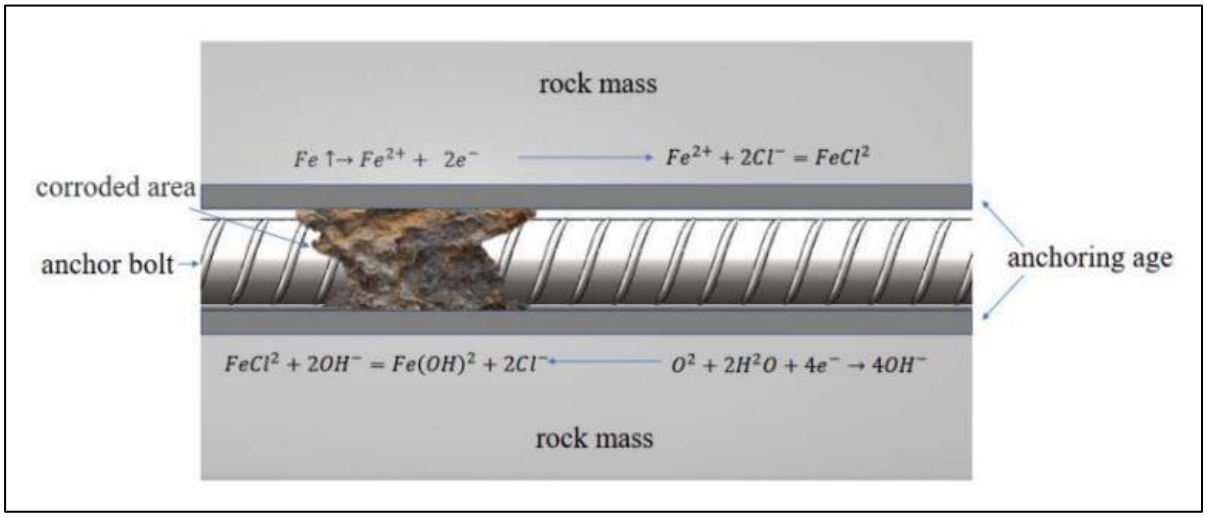

Figure 3. Schematic of anchor bolt corrosion [10].

As shown in Figure 3, when anchor bolts are used for a long time in environments with high chloride ion content, they are prone to corrosion by chloride ions. The evolutionary process of anchor bolts being corroded by chloride ions is as follows [10].

1) **Initial stage**: Chloride ions infiltrate the interior of the anchor bolt anchoring system, eroding the surface of the anchor bolt and gradually breaking down the protective layer of the anchor bolt.
2) **Accelerated stage**: The deterioration of the protective layer on the surface of the anchor bolt intensifies, resulting in an increased exposed area of the anchor bolt. Chloride ions continuously penetrate and migrate, further corroding the anchor bolt.
3) **Stable stage**: The sectional area of the anchor bolt reaches a certain extent, causing a reduction in the cross-sectional area of the anchor bolt and resulting in a loss of the load-bearing capacity.

Due to the slow corrosion rate in natural environments, electrochemical corrosion methods are commonly used to accelerate the corrosion process [11]. The following reactions describe the principles of electrochemical corrosion.

Anodic reaction:

$$Fe \uparrow \rightarrow Fe^{2+} + 2e^- \quad (1)$$

Cathodic reaction:

$$O_2 + 2H_2O + 4e^- \rightarrow 4OH^- \quad (2)$$

The equation for the secondary reaction occurring in the anodic region is

$$Fe^{2+} + 2OH^- \rightarrow Fe(OH)_2 \quad (3)$$

Unstable $Fe(OH)_2$ will continue to oxidize in a humid environment and form $Fe(OH)_3$ in the following reaction:

$$Fe(OH)_2 + O_2 + 2H_2O \rightarrow 4Fe(OH)_3 \quad (4)$$

The presence of chlorides increases the hygroscopicity of anchoring agents, decreases their resistivity, and accelerates the corrosion of anchor bolts. Free chloride ions combine with the passive film on the surface of steel reinforcement to form water-soluble complexes, which react with alkaline substances to generate iron hydroxides and release chloride ions.

Chloride ions act as catalysts in this process. The chemical reaction can be represented by the following equations:

$$Fe^{2+} + 2Cl^{-} \rightarrow FeCl_2 \quad (5)$$

$$FeCl_2 + 2OH^{-} \rightarrow Fe(OH)_2 + 2Cl^{-} \quad (6)$$

2.3 Types of corrosion in rock bolts

In the choice and design of rock bolts, the corrosion factor is of exceptional importance[12]. Indeed, its impacts are considerable on the durability of rock bolts. Precisely, corrosion has been reported to have significant effects on the life of rock bolts, and their unanchored length is more vulnerable. In fact, in rocks surrounding deep tunnels, rock bolts often face aggressive environments such as high temperatures, high groundwater pressures, etc.

Rock bolts can be exposed to different forms of corrosion [13] such as:

1) **Uniform corrosion**: The uniform corrosion is either atmospheric corrosion of metal exposed to air and its pollutants or galvanic corrosion due to electrolysis media.
2) **Pitting corrosion**: is highly localized corrosion occurring on a metal surface. Pitting is marked by the development of sharply defined holes “pits”. Pitting corrosion occurs as a process where the metal loss is accelerated by the presence of a small anode and a large cathode. Pitting corrosion is a dangerous form of corrosion as it can cause failure where only small weight loss of metal is observed
3) **Stress corrosion**: Corrosion fatigue is the process in which a metal fractures prematurely under conditions of simultaneous and repeated cyclic stress loading. This is likely to occur at lower stress levels with fewer cycles than would be required in the absence of the corrosive environment. Stress corrosion is a progressive development and growth of brittle cracks in a metal due to the combined effects from localised corrosion and tensile stress.

Of all the types of corrosion, pitting is particularly dangerous as it removes capacity for the bolt to deform with strata movements. Sudden failure of a bolt is likely to occur when pitting corrosion is experienced. The type and nature of corrosion depend on the nature of the ground condition and bolt encapsulation. Generally, the type of corrosion and severity of the corrosion varies along the bolt.

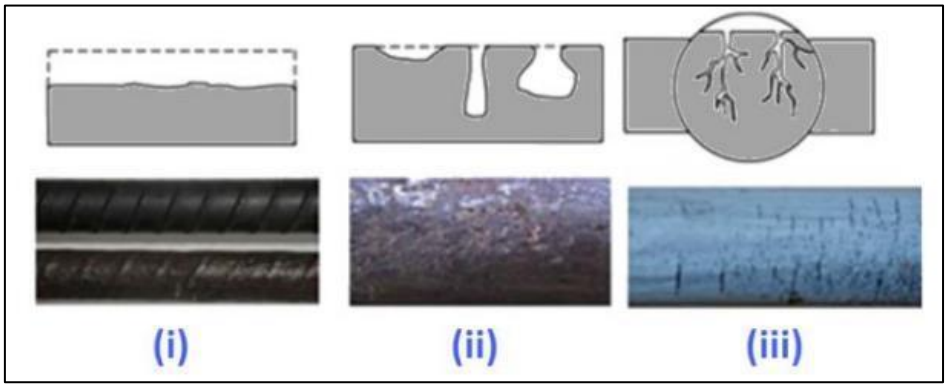

Figure 4. Illustration of corrosion in rock bolts, from left to right: (i) uniform corrosion, (ii) pitting corrosion and (ii) stress corrosion[12].

3 Non-Destructive Testing (NDT) of rock bolt corrosion

Rock bolts represent a critical element for many rocks mass stabilization, tunnel construction, and underground work projects. Therefore, the evaluation of their condition is vital for proving their functionality over the entire life cycle of structures. A number of techniques for quantifying condition of rock bolts are presently applied or are being developed.

A destructive method known as the pull-out test has been widely used in practice for determining capacity of installed rock bolts and assess their condition. Two types of pull-out tests can be conducted.

1) The first type is used to check the actual rock bolt capacity during which rock bolts will fail and be completely pulled out of rock mass.
2) The second test, the so-called proof load test, is used to verify if rock bolts can withstand load as foreseen in the design.

The pull-out method involves application of a gradually increasing tensile force on the exposed end of the installed rock bolt using a hydraulic jack, and determination of the force - displacement relationship, Figure 5. During the testing phase, the imposed force is measured by means of a load cell, while displacement values are measured by displacement gauges.

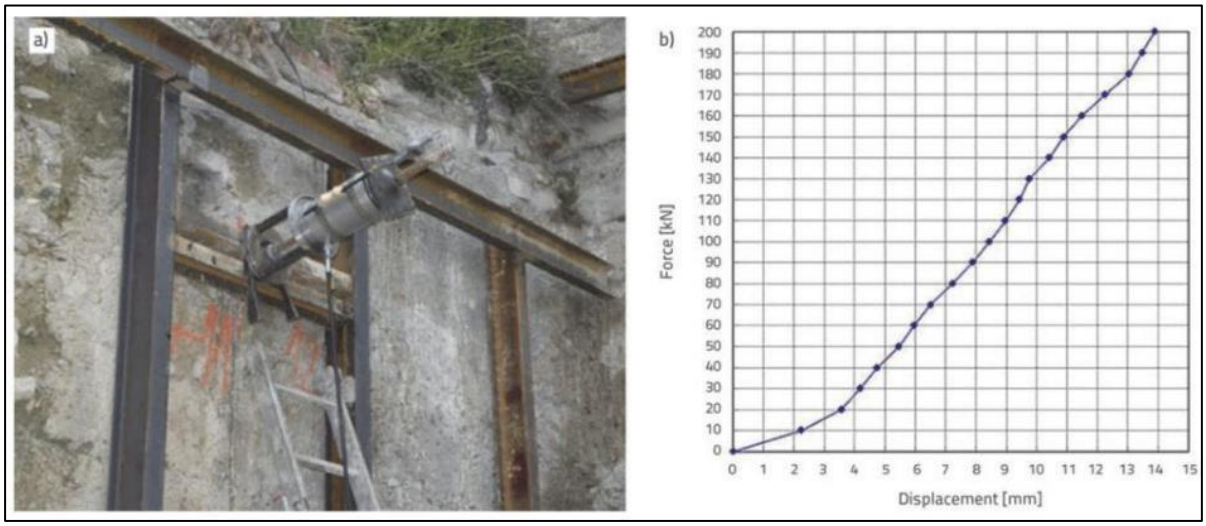

Figure 5. Pull-out test resulting force-displacement graph of so-called proof load test [14].

Non-destructive testing (NDT) methods can effectively assess corrosion in rock bolts without damaging them. Techniques like ultrasonic guided waves, acoustic emission, and electromagnetic are used to detect corrosion, evaluate its extent, and estimate potential future corrosion rates.

3.1 Electrochemical Open Circuit Potential (OCP)

Open Circuit Potential (OCP), also known as open circuit voltage, zero-current potential, corrosion potential, equilibrium potential, or rest potential, is a passive measurement method. It is commonly used to determine the resting potential of a system, serving as a basis for other experimental procedures. In certain tests, such as impedance spectroscopy (EIS) or Linear Polarization Resistance (LPR), the potential is referenced against the Open Circuit Potential (OCP) rather than a standard reference electrode. Consequently, a potentiostat can function as a straightforward voltmeter, measuring the potential difference between two points. The Open Circuit Potential (E_{OCP}) is simply the potential difference between working electrode (E_{WKG}) and reference electrode (E_{REF}).

$$E_{OCP} = E_{WKG} - E_{REF} \tag{7}$$

Therefore, a potentiostat can be used as a simple voltmeter, to measure the potential difference between two points.

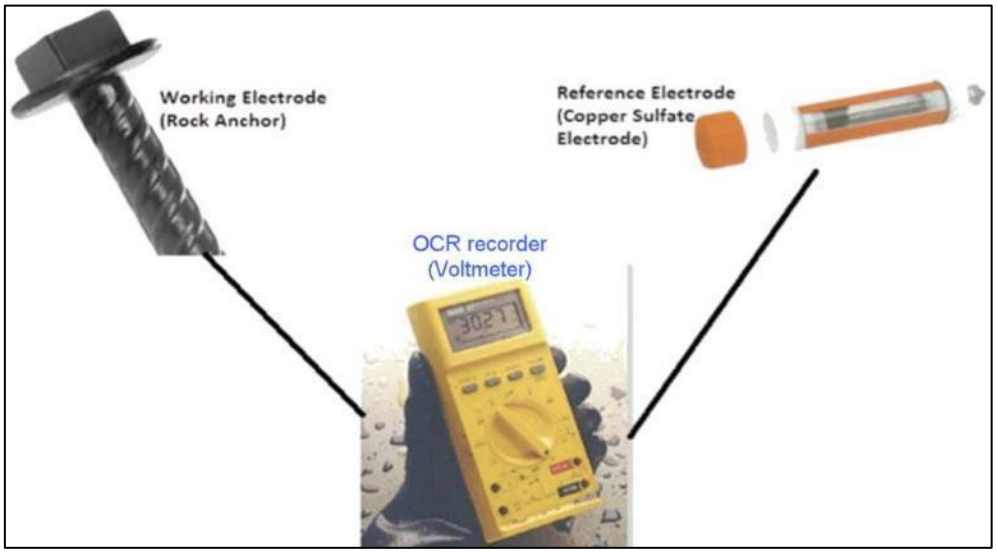

Figure 6. In situ open circuit potential measurement schematic [15], [16].

The following equipment, as shown in Figure 6, are needed for the measurements when taking the Open Circuit Potential (OCP) readings:

1) A voltmeter with the connecting cables that has a measurement range of 3.2 volts maximum and an accuracy of 0.001 volts.
2) A standard copper sulphate electrode (reference electrode).
3) Connecting wires with known resistivity.

Measurement Procedure

OCP voltage readings between rock bolt type and rock surface are taken by establishing the circuit shown in Figure 7. The multimeter is used to measure the voltage between a rock bolt and the reference electrode. Open Circuit Potential (OCP) voltage measurements are

recorded for different rock bolt types (if used) and for different rock surface conditions (wet and dry areas). Corrosion is obviously more likely to be severe in wet areas.

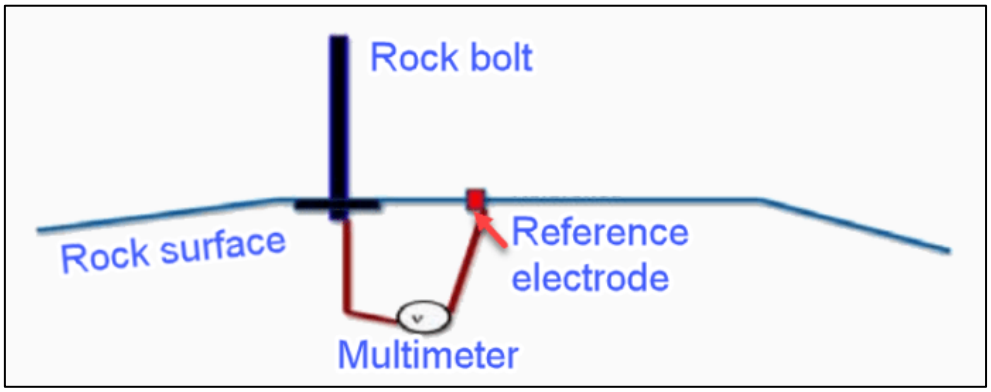

Figure 7. Simple schematic for Open Circuit Potential (OCP) potential readings from rock bolts.

Examples of Open Circuit Potential results

Open Circuit Potential readings of the Grade 60 steel roof bolts, which were collected from an underground coal mine and classified according to the three moisture conditions:

1) **Dry** –no sign of moisture was observed (0 – 60% RH)
2) **Humid** –the roof was slightly moist due to humidity in the mine atmosphere. Relative humidity greater than 60% was recorded as 'humid'. If the relative humidity values were less than 60%, the roof condition was recorded as dry.
3) **Wet** – water was visible on the roof and or dripping

Figure 8 shows 7 roof bolts potential data from dry, humid, and wet areas. All the bolts tested were older than 2 years. From the results, it was evident that the potential values are lower in a dry roof than in the humid and wet areas. The higher the potential value, the more corrosion-prone is the area. By comparing those values with the corrosion potential (Ecorr ≈ -500 mV) value of the steel bolts can be compared.

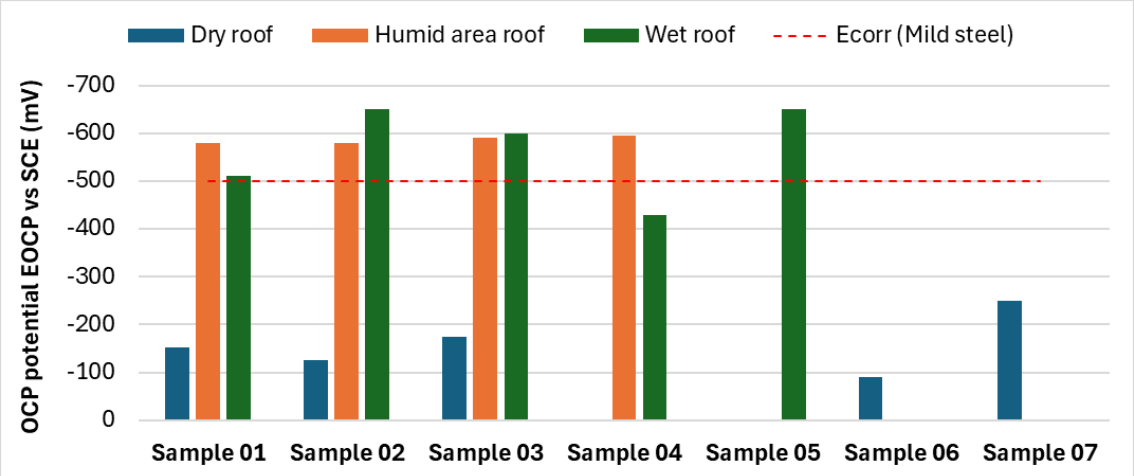

Figure 8. Corrosion potential determination chart with Open Circuit Potential (OCP) and E_{corr} comparison [16].

3.2 Ultrasonic pulse-echo

Ultrasonic pulse-echo is one effective way of evaluating the condition of these anchors. In this method, the transmitter and receiver (normally a one-piece transducer) are placed at the tip of the anchor bolt. In this context, pulse-echo requires very small access surface, which makes it ideal for testing anchor bolts. Ultrasonic pulse is then applied to the tip of the anchor bolt. The pulse travels along the length of the anchor (a specified range of frequency is used for practical considerations). The wave is reflected from the other end of the anchor, or any anomalies (including cracks and discontinuities) along the anchor length. The reflected pulse is received by transducer at the tip of the anchor. The time difference between the arriving reflections is used to locate the anomalies [17].

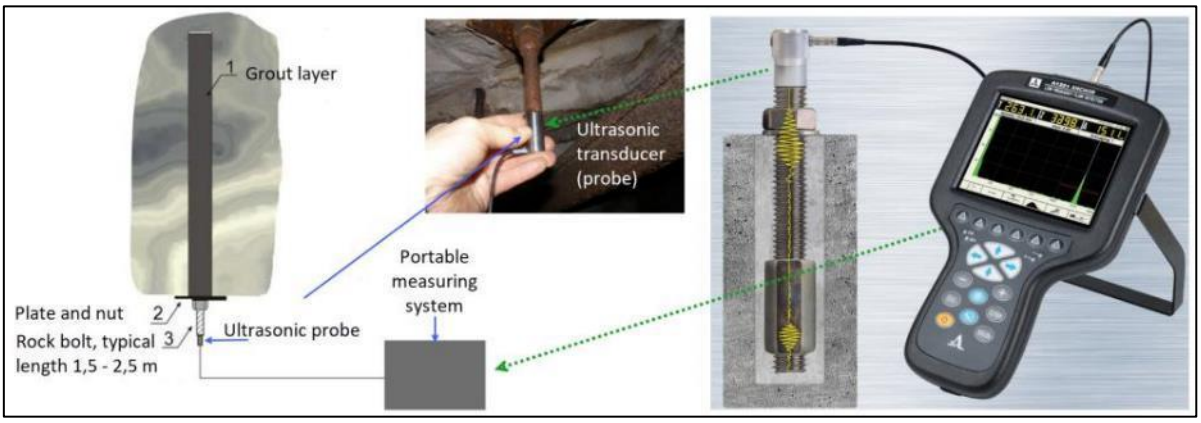

Figure 9. Experimental setup for ultrasonic measurements [18].

The data acquired from these bolts were in the form of unprocessed radio frequency (RF) signals in A scan. These A-scans illustrate the ultrasonic sound wave propagation within the bolts. When ultrasonic waves encounter a change in the material properties, such as a defect, they are reflected as echoes. These echoes are analysed for their time-of-flight and amplitude data. The data obtained from these echoes form the basis for categorizing defects. A sample of the ultrasonic A-scan signal from a thinning bolt is shown in Figure 10.

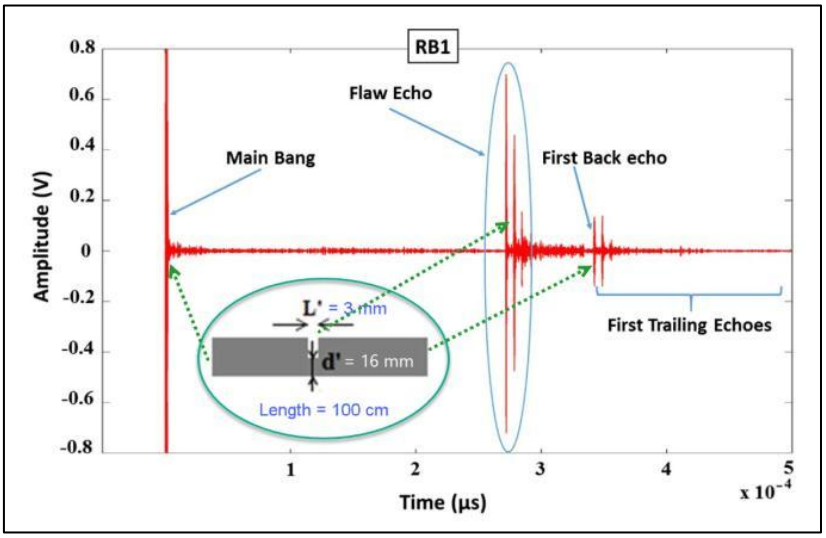

Figure 10. Characteristics of an ultrasonic A-scan signal [17].

A time-domain along with a frequency-domain analysis is applied to detect anomalies and deficiencies (such as corrosion defects, cracks); and to find out about the average cross section decreased due to corrosion.

- The A-Scan is a one-dimensional presentation of time versus the amplitude on the ultrasonic test machine screen.
- A-Scan shows the existence of flaws (if any present during scanning), and their position, and gives an estimate of their sizes.
- Time vs. amplitude, as shown in the Figure (left side), is the most efficient way of revealing the discontinuities.
- A-Scan displays the response along the path of the sound beam for a given position of the probe. It also displays the amplitude of the signal originating from the discontinuity as a function of time on the screen.
- The discontinuity depth (back wall echo) and time of flight are shown on x-axis. The 'y' axis indicates the amplitude of reflected signals (echoes) and can be used to estimate the size of a discontinuity compared to a known reference reflector.

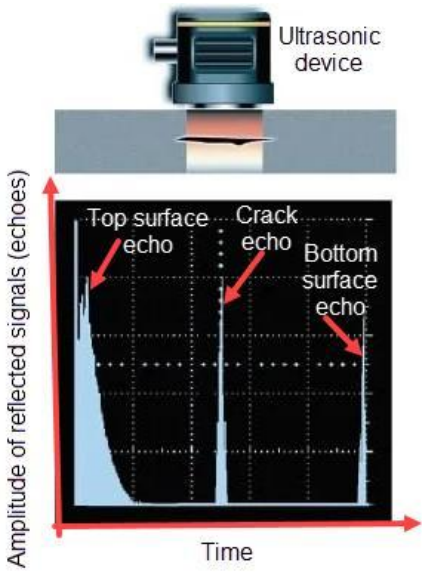

Figure 11. A-Scan Display in Ultrasonic Testing.

3.3 NDT with Guided Ultrasonic Waves

Guided waves are structure-borne ultrasonic waves that propagate along a structure confined and guided by its geometric boundaries. As shown in Figure 12, an application tailored ultrasonic transducer, excited by high-energy pulses from the instrument, generates elastic waves that propagate in the steel bolt embedded in grout. The waves propagate along the bolt, and a part of their energy leaks to the grout. An echo formed by the reflections from the discontinuities in the bolt (e.g., air packets or corrosion) as well as at the bolt end, is received by the sensing element of the transducer. Inspection relies on the principle that good grouting will absorb most or all of the wave energy into the rock, leaving only small echoes to reach

GWT is a technique for finding defect location and estimating the defect size using the arrival time and the amplitude of ultrasonic signal, respectively. The operating frequency of GWT is usually low (5 to 250 kHz) compared to ordinary ultrasonic testing. The low frequency operation helps to generate non-dispersive ultrasonic guided wave and to reduce the attenuation for long-range pipeline inspection.

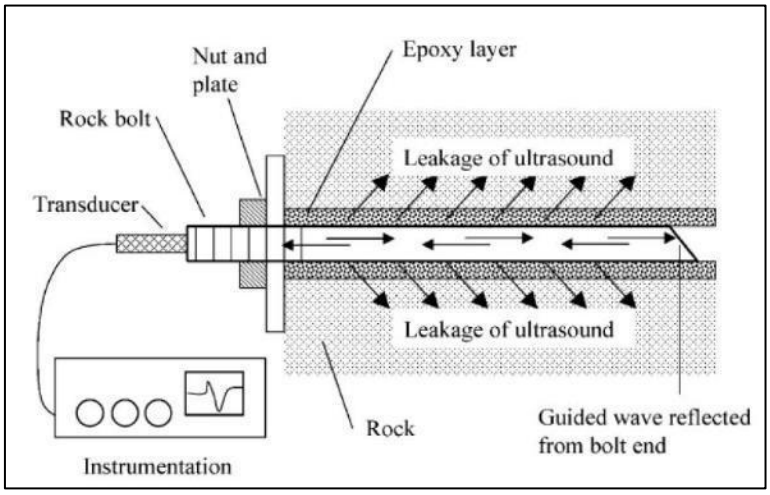

Figure 12. Schematic diagram of the rock bolt installation using guided waves inspection.

If a pulse of a guided wave propagates through a bar, the dispersion effect will cause its deformation, i.e. the pulse will be stretched in time, and its envelope will become elongated. The longer the propagation length, the more pronounced the dispersion effects will be. Guided waves have an important advantage - they can travel over long distances through pipes, bars and plates.

Guided waves are multimodal and dispersive, which means that, during propagation, a number of wave modes can propagate simultaneously with different velocities that are frequency dependent. The basic modes encountered in bars and tubes are compressional (Comp), torsional (T) and flexural (F) modes.

During the propagation of guided waves, there are three modes of waves: $L(0,m), T(0,m), and\ F(1,m)$. Here, 'm' represents the mode order, while '0' and '1', respectively, denote symmetric and asymmetric wave fields. The dispersion curves of a 20 mm diameter anchor bolt are shown in Figure 13. From the dispersion curves, it can be observed that within the frequency range of 0–1000 kHz, the $L(0,1)$ mode exhibits a frequency band with the fastest group velocity and minimal variation, spanning from 20 to 40 kHz. This characteristic enables the $L(0,1)$ mode to arrive at the receiving sensor first among all echo signals, without waveform distortion, making it easily identifiable and distinguishable in the time domain. Additionally, this frequency band falls below the cut-off frequency of other modal guided waves, thus ensuring that the $L(0,1)$ mode does not generate higher-order modal guided waves during detection[10].

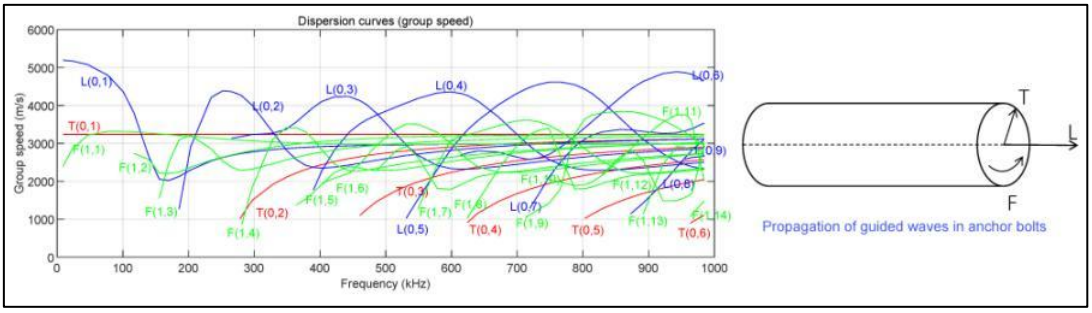

Figure 13. Example of the group velocity dispersion curve of 20 mm ribbed anchor bolts[10].

When guided waves penetrate the corroded area on the surface of a rock bolt, the reductions in the cross-sectional area and material damage in that region result in energy focusing and scattering, leading to changes in the distribution of energy density. Additionally, the propagation velocity and direction of guided waves within the rod are influenced by factors such as the properties of the medium and the geometric shape. Consequently, the change in the propagation path caused by corrosive defects also affects the velocity and direction of the wave propagation. The propagation of guided waves in anchor bolts with corrosive defects is illustrated in Figure 14.

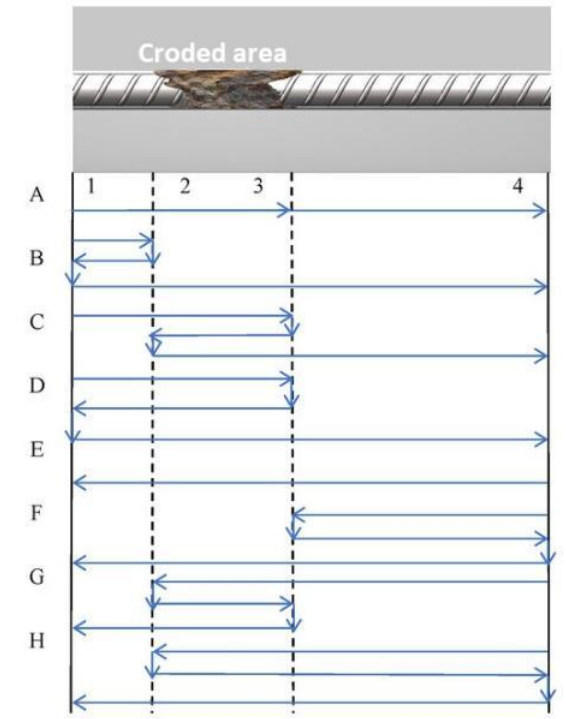

(A) wave transmission
(B) wave reflections at boundaries 2 and 1
(C) waves are reflected from boundaries 3 and 2
(D) wave reflections at boundaries 3 and 1
(E) wave transmission
(F) wave reflections at boundaries 3 and 4
(G) wave reflections from borders 2 and 3
(H) wave reflections from borders 2 and 4

Figure 14. Schematic of guided wave propagation [10].

3.3.1 Boltometer – Geodynamik AB

The Boltometer, developed in 1978 by Swedish company Geodynamik AB, uses a piezoelectric transducer to launch ultrasonic waves into the exposed end of the bolt and then measures the reflected signals. The ultrasonic waves are reflected from the end of the bolt or any discontinuities in the tendon itself and the discontinuities in the grout-tendon interface. The Boltometer can generate both compressional (P-wave), which is mainly used to determine the tendon length, and flexural/shear (S-wave) wave modes, which are reflected from the grouting discontinuities. The compressional wave is excited at a frequency of about 50kHz and the flexural wave at about 30kHz.

The non-destructive testing of rock bolt grouting quality using the Boltometer (Figure 15) started in 1983 with development of the first version of the apparatus. The Boltometer consists of the following main components:

- **Sensor** – The sensor contains several piezo-electrical crystals (divided into 4 sections), four light-emitting diodes (which indicate contact between the end of the

bolt and the four different sectors of the sensor) as well as a push button for starting the measuring procedure.

- **Main control box** – The main control box consists of a panel, electronics for generating, receiving and analysing the signals, as well as rechargeable batteries. The first Boltometer only showed the length of the bolt and an indication of its class. The instrument could however be provided with a mini oscilloscope for a more detailed study of the measured signal trace.
- **Supporting equipment** – For recording the complete signal trace, one could either attach a special printer or a separate memory oscilloscope with computer drive.

Figure 15. Boltometer instruments for non-destructive testing of rock bolt embedment [19].

Operating principle of the Boltometer

The Boltometer uses a sensor with piezoelectric crystals, which both generates and receives waves at the rock bolt head (Figure 16). The generated waves travel through the installed element, and, after reflection, they are recorded. The testing procedure is quite simple - if the rock bolt is well grouted, the energy return will come only from the rock bolt end. However, if there are any anomalies in the grouted section of the rock bolt, a certain amount of energy will be reflected from the anomaly, and it will be registered as such on the rock bolt head.

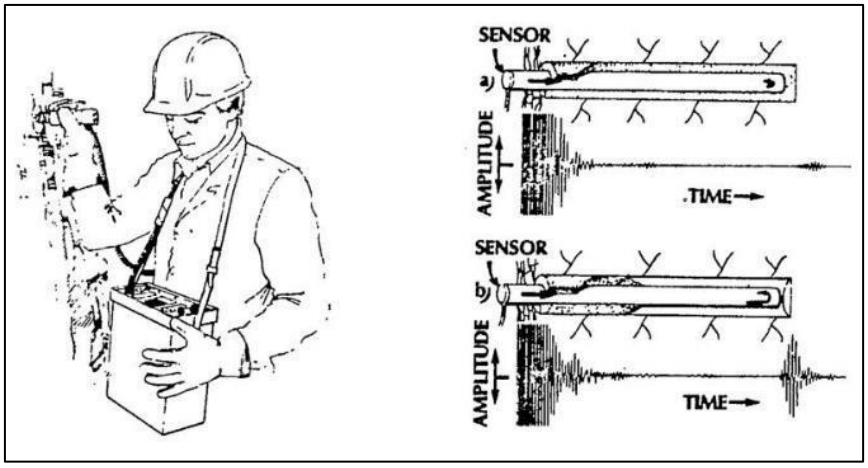

Figure 16. Diagram and operating principle of the Boltometer [20].

If one analyses the time signature in the waves which have passed through the bolt and which have been recorded or registered from the bolts outer end one finds that the waves are influenced in different ways all relative to the condition of the bolt, the grout and the rock. In an undamaged well grouted bolt (Figure 17) a great deal of the wave's energy is emitted to the surrounding rock because the contact with the rock is very good. Hence on the recording of the reflected wave a very small "echo" or no "echo" at all may be had from the inner end of the bolt [21].

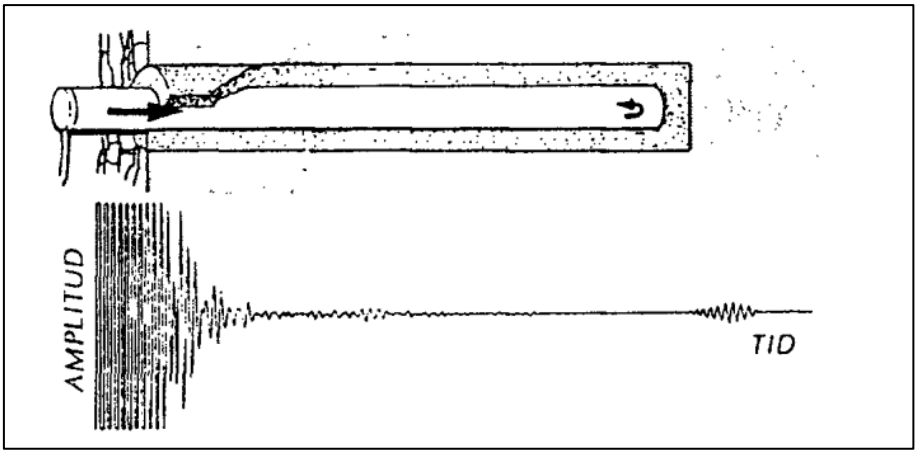

Figure 17. Undamaged well grouted bolt.

If the grouting is of poor quality or if the grouting along a portion of the bolt is missing (Figure 18) the wave's energy is less damped, resulting in a stronger echo.

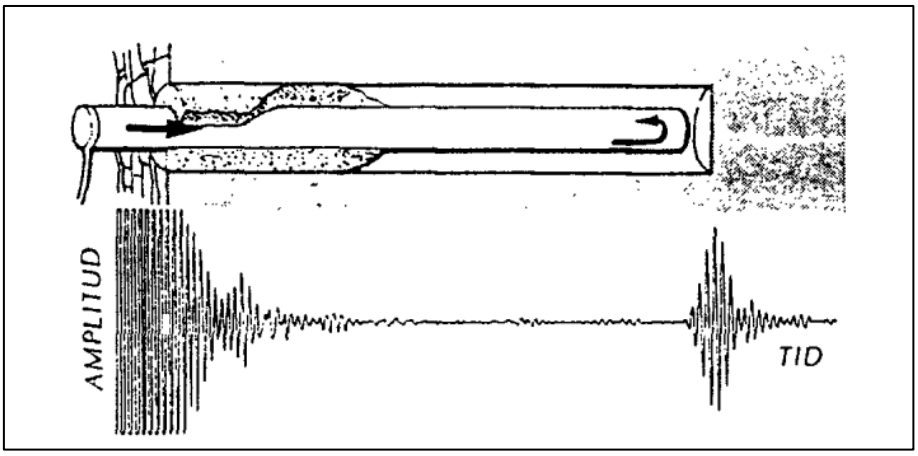

Figure 18. Defective grouting.

The size of the echo (signal amplitude) thereby indicates the bolt's quality:

- a small echo = good quality.
- large echo = poor quality.

Damage to the bolt, i.e. a crack, rust formation or a heavy bending (Fig. 5) will create a partial echo which depending on the extent of the damage, can be distinguished more or less clearly in the measured signal.

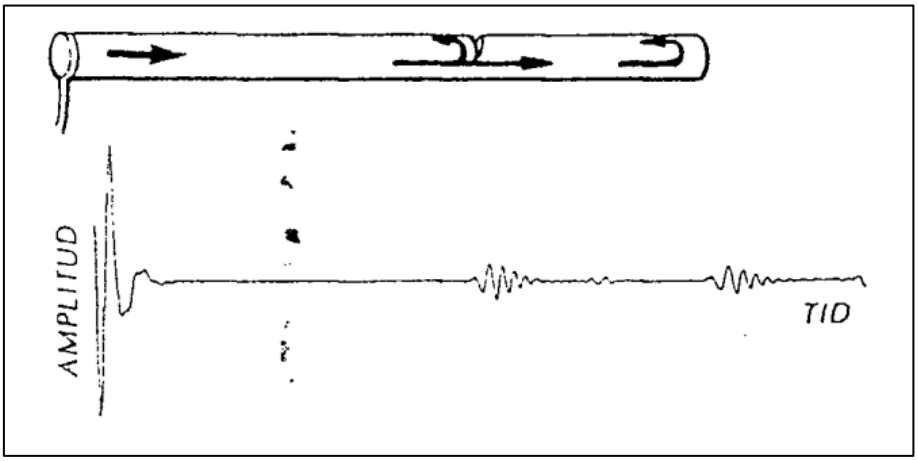

Figure 19. Defective bolt.

The Boltometer makes use of both compressional (primary or P) and flexural/shear (secondary or S) wave modes, and the transducer set is carefully designed to separately stimulate and measure each type of wave.

P-waves (compression waves) typically travel faster than S-waves (shear waves) through both steel and rock. In steel, P-waves travel around 5,9 km/s, while S-waves travel around 3,1 km/s. In typical crustal rocks, P-wave velocities range from 3.0 km/s to 6.5 km/s, while S-wave velocities range from 1.5 km/s to 3.8 km/s.

An annotated typical recorded Boltometer test result is shown in Figure 20.

1) The first line shows the date and time.
2) The second line shows the class and sensor information: four LEDs that show how well the sensor is in contact with the bolt.
3) The third line shows the measured length of the bolt.

The compressional waves are excited at a frequency of about 50 kHz and are reflected by the inner end of the bolt but are generally not particularly diagnostic of discontinuities in the grout. They are used primarily to detect the effective length of the bolt by measuring the time delay of the end echo and multiplying this by the velocity of sound in the bolt [26].

The flexural/shear waves are excited at a frequency of about 30 kHz and are a distinguishing characteristic of the Boltometer: no other acoustic technique reviewed made deliberate use of this propagation mode. The flexural waves are also reflected by the inner end of the bolt, but more importantly, they are sensitive to the quality of the grout and echoes can be seen at grout discontinuities. They are also less heavily attenuated than the compressional waves, and consequently they allow the instrument to make meaningful measurements on longer bolt than would be the case if only compressional waves were used [21].

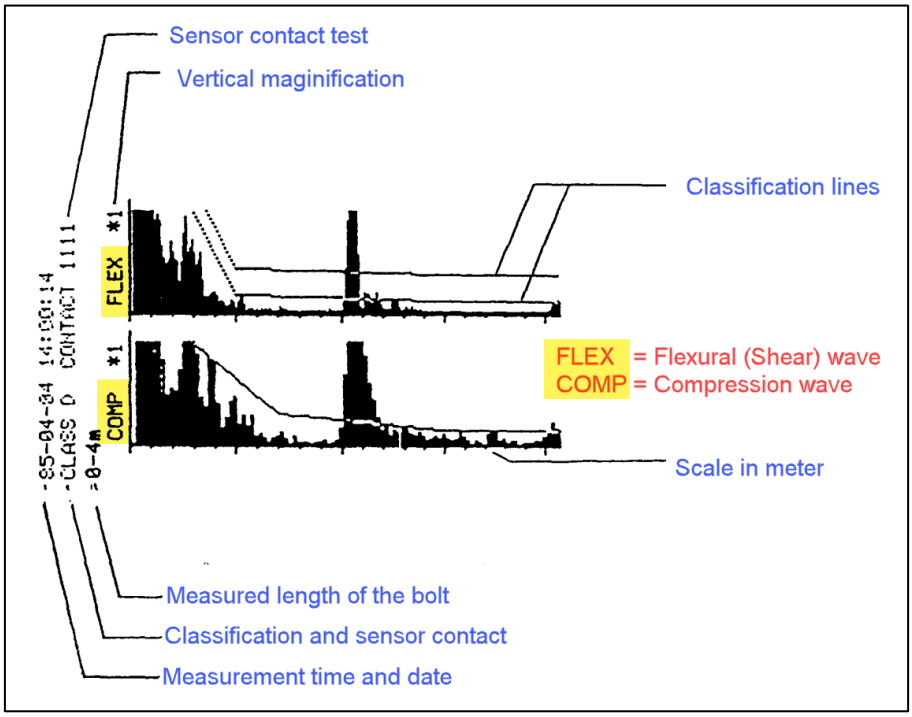

Figure 20. A typical Boltometer result[14].

The main principle behind the instrument's determination of grouting effectiveness is in fact the simple one of energy absorption:

- if a bolt is well grouted, and hence well coupled to the rock throughout its length, most of the acoustic energy will be transmitted through the grout and dispersed in the surrounding rock, and very little echo will be seen in the recording of received signal vs. time.
- On the other hand, significant gaps in the grouting will not only provide interfaces against which the waves can reflect but also absorb less of the available reflection energy.

Consequently, the Boltometer classifies grouted tendons into four classes: A ("optimum"), B ("reduced"), C ("deficient") or D ("very poor"), based upon the level of echo energy observed in the recording. The flexural wave response is more important for this classification than the compressional wave.

- **A: Optimum** – Fully grouted, being continuously grouted rock bolt with good quality grout.
- **B: Reduced** – Some defects in grouting, often accepted
- **C: Deficient** – Poorly grouted
- **D: Very Poor** – Very poorly grouted, being a rock bolt with significantly reduced grouting quality.

Reference bolts

When a Boltometer is delivered certain parameters (principally the Comp-wave and Flex-wave seismic velocity and pulse frequency) are preset by means of the pre-delivery test

applied to each instrument. The pre-delivery test is carried out on approximately 2 m long bolts of rebar with a diameter of 25 mm cement grouted into 38 mm diameter boreholes drilled into fairly solid granite.

If the Boltometer is used under deviating circumstances - i.e. with smaller or larger bolts and/or borehole diameters, poorer rock or alternative grouting material - the preset parameters may need to be adjusted relative to existing conditions. This is done simply and most reliably with the aid of reference bolts.

The aim of the reference bolt is to determine under existing conditions in certain mine or underground works:

1) The measurement range of the Boltometer (penetration ability)
2) Classification limits for relative area of investigation.

For this purpose, a suitable rock area of average quality with respect to frequency of cracks etc; should be selected from the works. Within this area of the rock, a number of holes are drilled using standard drill equipment and having a variety of lengths (1,0 - 2,5 m increasing by 0,25 m for bolt lengths of approximately 2,0 m). It is suggested that two holes are drilled of each length together with four extra holes of standard length. One of every two holes are drilled downwards at an angle.

A standard bolt is fixed into each hole drilled (standard diameter, standard drill equipment, cement grouting with standard water/cement ratio). The above mentioned four extra holes are intended for bolts with only 40 cm depth of grouting from the surface of the rock. This simulated inferior grouting is achieved by either placing a manchett around the bolt or by filling the inner portion of the hole with Styrofoam. All bolts are chopped off 10 cm outside the rock surface: the exact length of each bolt is noted. If the cutting off does not finish off in an absolutely level plane the end of the bolt is ground flat.

In order to create boundaries for the different classes of function (Figure 21), all the reference bolts are measured and documented.

- The dividing line between Class A and Class B is created by making the limiting line 1 for the Flex-wave slightly higher than that of the Flex-wave echo from the bolt end for the bolt which corresponds with local requirements for “well grouted bolt”.
- The limiting line between Class B and Class C is created by placing the limiting line 2 for the Flex-wave at a position which corresponds to the position of the limiting line 1 plus 50%.
- The limiting line between Class C and Class D is created by placing the limiting line for the Comp-wave at a position which corresponds to the Comp-wave echo for a bolt having less than 30 cm of good grouting.

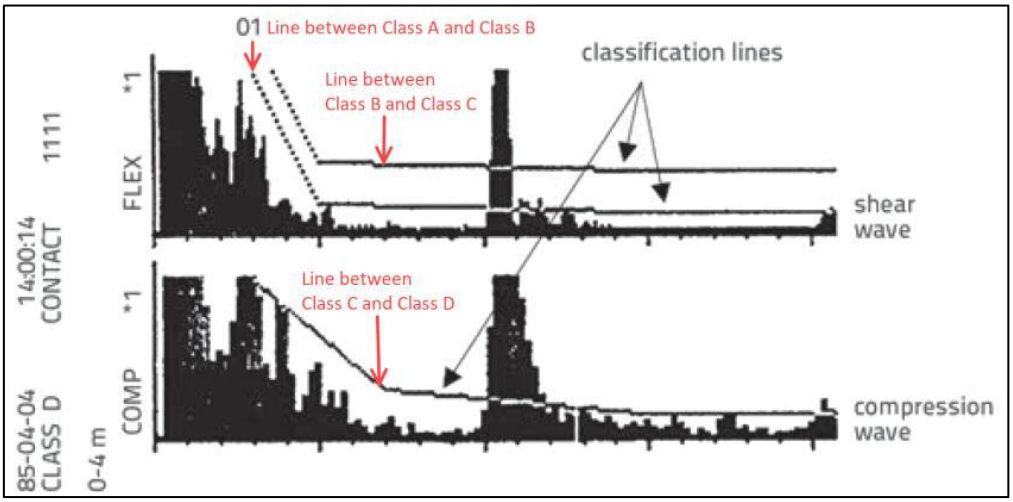

Figure 21. Boltometer boundaries for the different classes.

Interpretation of the Boltometer results

To classify the investigated rock bolts into one of the classes, the Boltometer uses reference classification lines, through which the returned signal is evaluated.

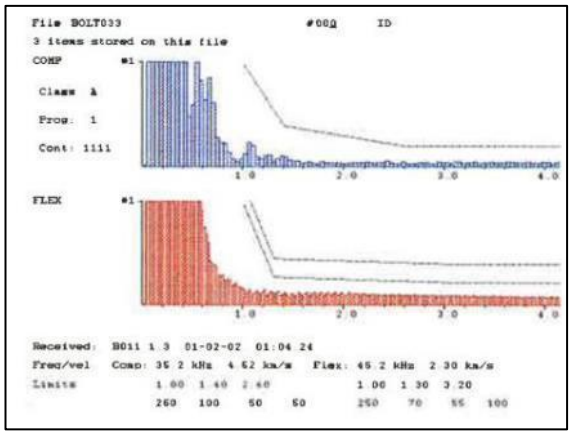

Class A – Optimum

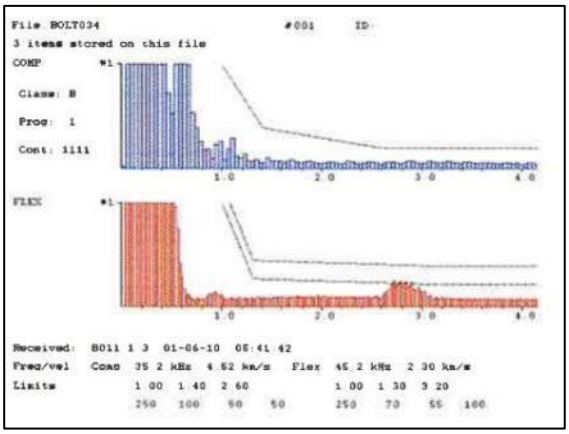

Class B – Reduced

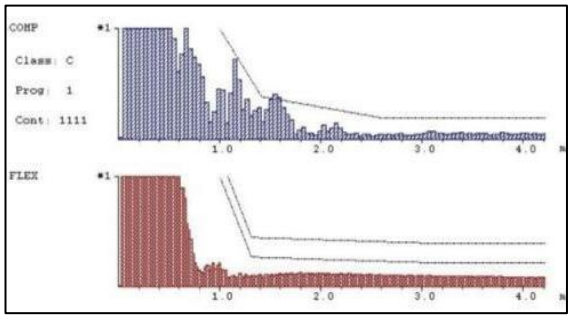

Class C – Deficient, poorly grouted

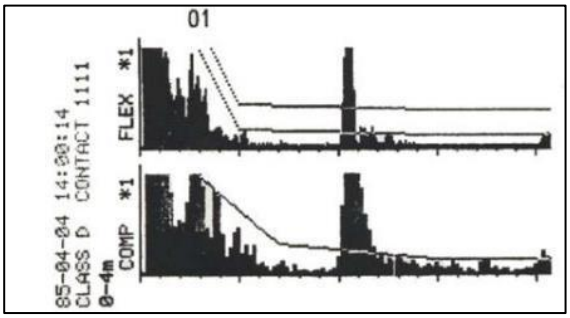

Class D – Very poorly grouted

Figure 22. Examples of the Boltometer measurement results.

In general, proper interpretation of results requires professional skills, great care, a lot of reliable information about calibration bolts and sufficient knowledge of how to use the Boltometer device.

- There are two graphs, compression (COMP) and flexural (FLEX) waves.
- The x-axis shows the length, the y-axis shows the amplitude of the reflected wave, or "echo", "*1" indicates the amplitude strength.
- The lines in the graphs are classification lines based on the data obtained from the calibration bolts. If the amplitude exceeds the line, the classification becomes worse. The basic principle can be considered that the flatter the diagram, the better the classification and therefore the more successful the bolting.

Examples of the Boltometer measurement results of different classification classes are presented in Figure 22.

Measuring in the field

The Boltometer's own sensor is held against the free end of the bolt (Figure 23). The Boltometer sends a wave motion to the bolt, part of whose energy is transferred to the solder and part to the rock, reducing the original amplitude of the wave. After reaching the end of the bolt, the wave is reflected back. These reflected waves can be read with the same sensor. If the grouting around the bolt is successful, or covers the entire bolt completely, the amplitude reduction is large. That is, the better the grouting, the smaller the amplitude of the reflected wave and the worse the grouting, the greater the amplitude. By analyzing the amplitudes obtained according to the calibration bolts, the grouting made on the construction site can be classified from A to D, where A is the best and D the worst. If the calibration has been performed correctly, the machine itself classifies the grouting being tested. Since the Boltometer also monitors time, it is possible to calculate from the results how deep the defect is in the bolt. In addition, the operating principle of the Boltometer allows the detection of mechanical defects in the bolt itself [22].

Figure 23. NDT of rock bolts by the use of guided ultrasonic waves: The Boltometer [19].

A test measurement of a certain rock bolt can be carried out in two different ways:

1) **Quick estimation**, where the intention is to determine as soon as possible whether the bolt in question is damaged or has defective grouting (primarily along the outer part).
2) **Comprehensive testing**, where the intention is to document the bolt installation as accurately as possible.

For quick estimation it suffices to hold the sensor only once against the plane outer end of the bolt and estimate the function and/or length of the bolt by either using the reading from the "bolt class" meter (A - satisfactory function, B = reduced, C = defective, D = insufficient) or by roughly estimating the signal on the LCD display (no echo = satisfactory function, occasional echo = defective, several powerful echoes = insufficient function).

In comprehensive testing, more conclusive measuring procedure in order to obtain more accurate results. To begin with an optimal contact must be created between the sensor and the bolt end, i.e. the bolt end must be carefully levelled by cutting or grinding and a certain amount of contact paste or acoustic gel applied. Secondly the optimum measuring signals should be attained by repeated measurements with the sensor in different positions.

- At the start of the measurement process, the maximum signal amplification ratio is set on the LCD display, specifically at 5:1.
- Then, the sensor is carefully pressed against the end of the bolt and aligned using the four sensor LEDs, which correspond to the sensor's four sectors. When all four LEDs are lighted up, an automatic measurement is taken.
- If no echoes are detected on either the Flex-wave or Comp-wave signals, the sensor is rotated by 30 degrees, and the measurement is repeated.
- If five different sensor positions are tested at an amplification of 5:1 without detecting any echoes, it can be concluded that the bolt's grouting quality is satisfactory, indicating no damage to the bolt or its grouting along its entire length, as determined by reference bolts.
- In cases where an echo is observed on either signal, efforts should be made to maximize the echo in the Flex-wave signal by adjusting the sensor orientation in 30-degree increments. The strongest Flex-wave echo should be recorded using the printer output. Strong and frequent Flex-wave echoes generally indicate poor grouting quality for the specific bolt.
- If the total grouted length is less than 50 cm, a Comp-wave end echo is likely to be visible; in such cases, attempts should be made to measure and record the largest possible Comp-wave end echo.

Disadvantages of the Boltometer [21], [23]

- The most critical shortcoming of the Boltometer in relation to the present problem is the instrument's inability to measure cable tendons. This is due to the fact that the instrument relies for its operation on a simple cylindrical model of the tendon. In cable tendons, the stranding results in an acoustic response which is too complex to interpret correctly.

- A second shortcoming is the need to ensure that the exposed end of the bolt is clear and unencumbered before Boltometer measurements are attempted. The presence of nuts, washers, and to some extent mesh, lace or shotcrete, causes problems as this results in a large portion of the acoustic energy disappearing into the rock via these peripheral support elements, rather than propagating along the bolt itself. In addition, for a reliable reading, the outer end of the bolt needs to be planar (cut and ground flat), and acoustic gel should preferably be applied to achieve good coupling between the sensor and the bolt end.
- A third practical impediment with the Boltometer is that, to obtain meaningful measurements, it is necessary to calibrate the instrument and optimise settings very specifically against the type of tendon installation to be measured. This requires installing reference bolt of the same type and length, using the same grout consistency, in the same type of rock as the target tendons. It is recommended that three such bolts of each combination be installed under carefully controlled conditions. Clearly this has cost and practicality implications for the use of the instrument but once having been carried out for a particular geotechnical environment, it does not have to be repeated.
- The need to calibrate against rock type arises because of the reliance of the Boltometer's shear wave mode on the grout waveguide effect. If the surrounding rock is about the same stiffness as the grout, much of the wave energy will dissipate into the rock, making end- or part-echoes difficult to see. For this reason, it can be impossible to distinguish between a poorly grouted tendon in soft rock and a well grouted tendon in stiff rock.

3.3.2 The Rock Bolt Tester (RBT)

The Rock Bolt Tester (RBT) instrument (Figure 24) applies long-range ultrasound to investigate bolt's status, especially its grouting condition. RBT features an application tailored ultrasound probe that transmits high-energy, low frequency (below 100kHz) guided waves and is capable of receiving weak echoes reflected from the discontinuities at the bolt surface as well its end-echo that have propagated in the range of up to four meters.

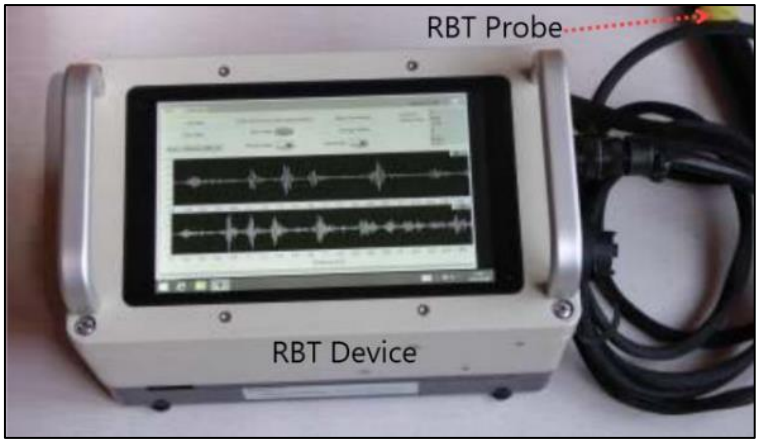

Figure 24. The Rock Bolt Tester (RBT) [19].

Measurement principles

The RBT instrument operates on the principle of ultrasonic guided waves that propagate in solid media limited by hard boundaries, for instance, plates, bars and tubes. Guided ultrasonic waves have a more complex physical behaviour than bulk elastic waves, i.e. longitudinal (L) and shear (S) waves, commonly used in NDT methods.

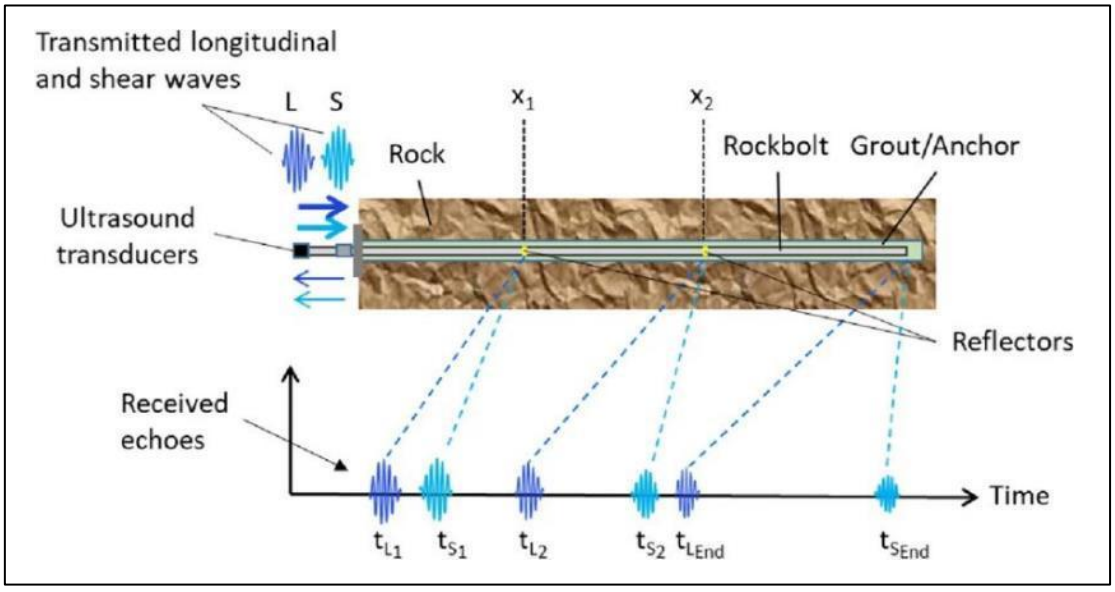

Figure 25. Longitudinal and shear ultrasonic waves are propagated along the rock bolt and time of flights of echoes reflected from discontinuities inside the bolt and the bolt end inside the rock are measured [24].

With reference to Figure 25, an ultrasonic longitudinal wave transducer and an ultrasonic shear wave transducer are mounted on the exposed end of a full-bodied rock bolt to propagate longitudinal and shear ultrasonic waves along the rock bolt. These waves will be reflected from the distal end of the bolt and eventually from inside reflectors as well and return to the transducers as echo signals. The transducer serves to emit and receive longitudinal and shear waves.

The time of flight (TOF) for a particular wave to travel the round-trip distance between the transducer and the distal bolt end or reflectors will depend on the travel distance, the temperature, the stress in the bolt, and the wave type (i.e., longitudinal type for waves of which the wave vibration is along the wave propagation direction, or shear (also called transverse) type for waves of which the wave vibration is perpendicular to the wave propagation direction).

It is to note that a rock bolt is an acoustic waveguide in which acoustic waves of different frequencies and vibration modes travel at different velocities. When operation frequencies of the longitudinal wave transducer are high enough, some modes of the generated acoustic waves will travel at high velocities with relatively low attenuations. An echo signal of such waves will arrive ahead of others. This is the echo signal that we use and refer to as longitudinal wave echo signal in this work. The centre frequency of shear wave transducer is selected in such a way that it is high enough to favour better spatial resolution but not too high to avoid excessive attenuation of the acoustic energy by the wave propagation medium [24].

Rock Bolt Tester (RBT) instrument

The Rock Bolt Tester (RBT) instrument (Figure 26) applies long-range ultrasound to investigate bolt's status, especially its grouting condition. The portable Rock Bolt Tester consists of:

1) **PC computer**, which contains specially designed digitally controlled electronic boards of signal generator and signal receiver connected as illustrated in the block diagram.
2) The boards are connected to the **Data Acquisition Card (DAQ)** card, which performs data communication and signal acquisition.
3) The programmable **pulse generator** can emit high-energy long pulse trains, for example, windowed chirp sequences. Two separate pulse sequences generate the compressional and quasi-flexural waves in the bolt.
4) The programmable **receiver** has two separate channels capable of amplifying small echo signals received by the mode sensitive probe.
5) The RBT's **probe** consists broadband piezoelectric stack actuators and sensors integrated into a single handle. The probe's actuators transmit elastic waves, possibly broadband compressional and quasi-flexural modes, into the rock bolt. An echo signal formed by the reflections from the discontinuities in the bolt is received by the mode-sensitive sensor part of the probe.

RBT features an application tailored ultrasound probe that transmits high-energy, low frequency (below 100kHz) guided waves. It is also capable of receiving weak echoes

reflected from the discontinuities at the bolt surface as well its end-echo, which have propagated back and forth in the range of up to 4 meters. The RBT is a portable instrument that consists of specially designed analogy electronics for generation and reception of guided waves and an embedded digital computer that performs for signal processing, operator communication and data storage. In the paper we will focus on advanced processing techniques applied to enhance tiny echo signals received by the probe [25].

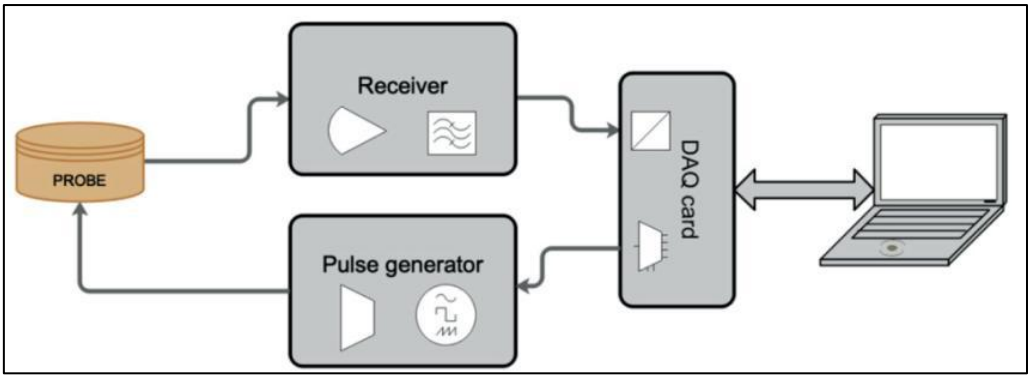

Figure 26. Diagram of the RBT instrument[25].

Measuring in the field and interpretation of the RBT results

The operator initiates the RBT measurement (Figure 27). Compressional and flexural waves are then transmitted in two separate pulses from the source to the bolt. The echo signal is received by the sensor and amplified before it can be viewed on the PC in real time [26].

Figure 27. NDT of rock bolts by the use of guided ultrasonic waves: Rock Bolt Tester (RBT) [19].

An example of the raw signals, registered for a partly grouted 2m long rock bolt is shown in the upper panels in Figure 28. It can be seen that the filtered signals, shown in the lower panel, feature much higher Signal-to-Noise Ratio (SNR) than the raw ones. The large pulses at 1 ms are the reflections from the bolt end while the small echo seen at 0.5ms is the reflection from the grout discontinuity [25].

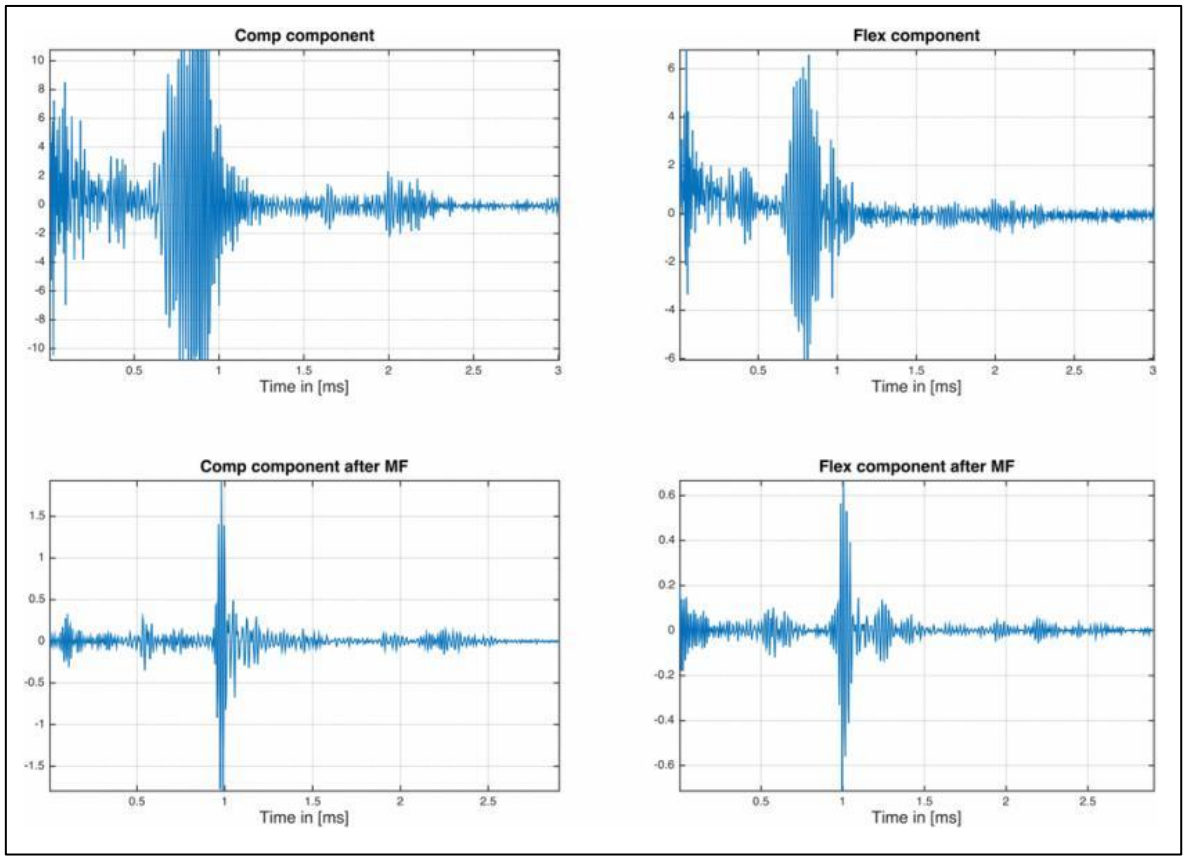

Figure 28. Example of ultrasound echo signals registered by the RBT instrument. Compressional component (left) and flexural component (right). Raw signals in the upper panels and the matched filter processed signals in the lower panels[25], [27].

Example of the experimental validation of the RBT instrument

The following example confirms the RBT's testing conducted across three tunnels in Sweden. The test locations were situated within tunnel projects beneath Stockholm and at the Dannemora Mineral AB mine in northern Uppland. At each site, 22 identical test bolts were installed using cement grout[27].

The method of creating an operational test bolt with artificial defects to evaluate techniques has been adopted from the NDT field. This approach relies on a set of representative cases believed to be applicable to a wide range of defects and deviations. In general, each flaw or deviation is unique, making it impossible to develop a test bolt that encompasses all possible variations.

The fundamental hypothesis behind the tests was that the most frequently occurring flaws result from either the failure to insert the pump hose into the bottom of the borehole or an

excessively high water-cement ratio, which causes the cement mix to slip out of the hole. In both scenarios, a cavity should form at the bottom of the borehole. While it is possible for the cement mix to escape from the outer section of the borehole and create a cavity there, such a defect would be easier to identify and likely cause less damage[27].

The test bolts were produced by covering a specific length of steel bolt with a plastic tube sealed with silicone, safeguarding this section from contact with the grout. The schematic diagram in Figure 29 illustrates the bolts used in the experiments, also showing that many bolts were fitted with plastic end caps to ensure consistent conditions for end echo measurements. These end caps isolate the bolt's end from the grout, thereby preventing energy leakage. Additionally, both energy leakage and wave velocity are influenced by the type of grout, specifically by the difference in acoustic impedance between the grout and the steel used in the rock bolts.

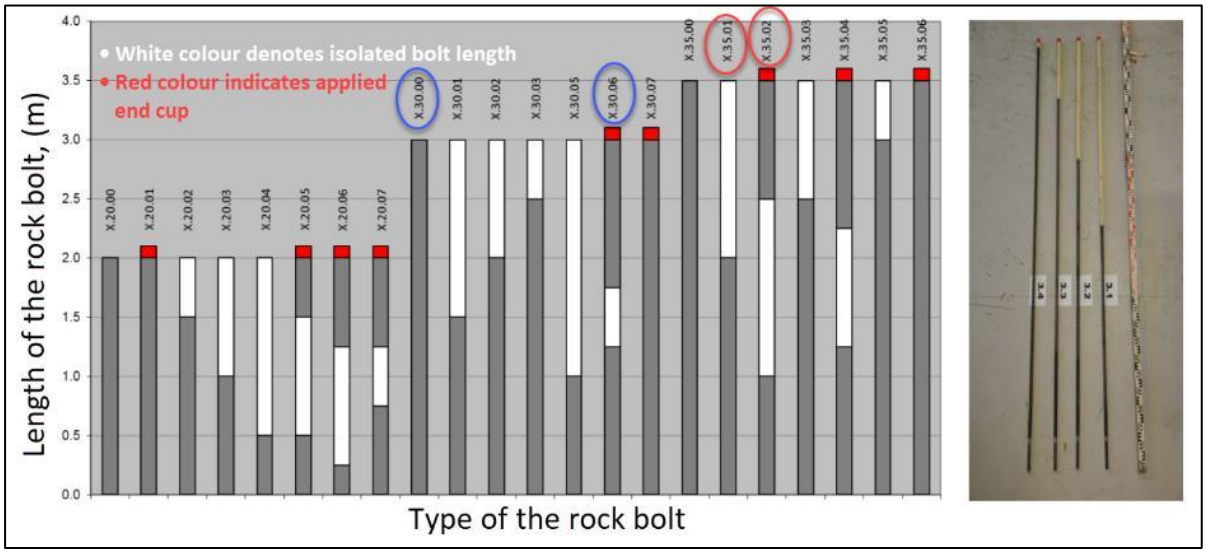

Figure 29. Schematic drawings of the prepared bolts used in the tests (left) and (right) the prepared bolts with end cups and plastic tubes [27].

Examples of the most representative results of the prepared rock bolts installed at the Dannemora Mineral AB mine are presented in Figure 30 and Figure 31.Both the longitudinal (L) and transverse (F) components are displayed as amplitude plots generated by the RBT's LabView software.

The A-scan amplitudes plotted on the y-axis are on an arbitrary scale, influenced by the instrument gain, the length of the test signal, and the digital filter settings (which remained constant throughout testing). The bolt length on the x-axis is calculated assuming an average wave velocity of 3.0 km/s.

Between October 2012 and November 2015, approximately 3200 tests were conducted. During each test, multiple measurements were taken for each bolt as the probe was rotated. These tests, which were repeated at various intervals following successive modifications to the probe, aimed to maximize the echo received from ultrasonic signals scattered at artificial discontinuities [27].

Example of A-scan signals recorded for two 3-meter bolts (X.30.00 and X.30.06) are shown in Figure 30, where clear end echoes for both bolts are prominently visible. Additionally, two echoes reflected from the 0.5-meter air pocket located midway along bolt X.30.06 are distinctly evident. It is also noteworthy that secondary echoes for bolt X.30.06 are more presented, likely due to reduced attenuation caused by the presence of the air pocket.

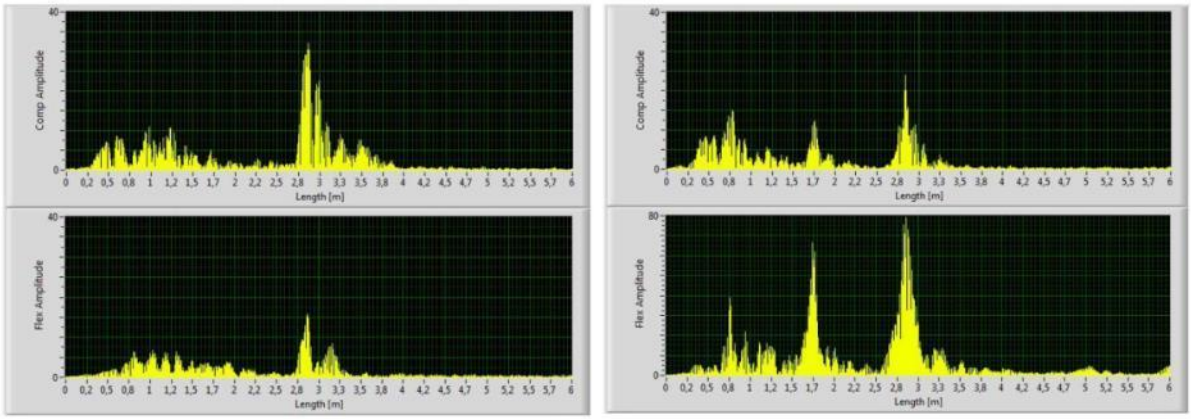

Figure 30. A-scans obtained for the bolt X.30.00 (perfect grout, no end cup, see Figure 29) (left), and the X.30.06 (0.5m tube in the middle, end cup) (right). Compressional component in the upper panels and the flexural in the lower panels.

A-scans from multiple tests of the same bolt, with the probe rotated, are shown in Figure 31. As observed in the figure, the presence of a void at the end of the bolt produces a stronger end echo compared to a similar void located in the middle of the bolt. This is reasonable because a void in the middle generates two distinct echoes, which reflect a significant portion of the wave energy back. In contrast, a void at the end reduces overall attenuation, allowing even the double echo at 7 meters to be distinguishable in the bolt labeled X.35.01. This indicates that the maximum effective testing range of the RBT instrument is at least 4 meters.

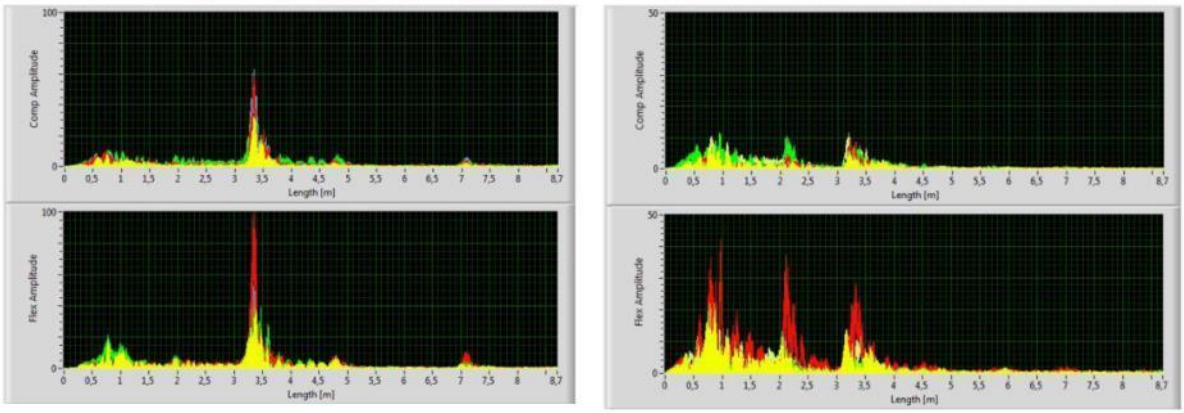

Figure 31. A-scans obtained for the 3.5m rock bolts. Left panel: bolt X35.01 (1.5m long tube at the end, no end cup). Right panel: bolt X.35.02 (1.5m long tube in the middle, end cup).

3.4 Electromagnetic waves method

Electromagnetic waves can be used to inspect the condition of rock bolts, particularly for detecting defects like non-grouted sections or voids. This method, often employing time-domain reflectometry (TDR), utilizes the reflection of electromagnetic waves to identify changes in the rock bolt's structure.

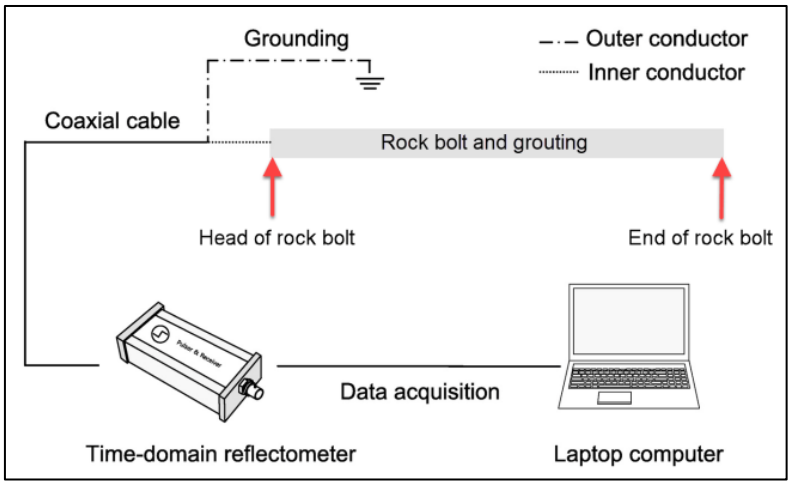

Figure 32. Measurement system and cable connection [28], [29].

An example of an electromagnetic wave measurement system is illustrated in Figure 32. The electromagnetic wave is generated and received using a Time Domain Reflectometer (TDR). The TDR produces a step pulse with an amplitude of 250 mV and a duration of 3.0 µs. The inner conductor and outer conductor of the coaxial cable are connected with the TDR to generate and receive electromagnetic signals. The coaxial cable is RG-58A/U, which is commonly used for low-power signal and radio frequencies. The impedance of the coaxial cable is 50 Ω. The inner conductor of the coaxial cable is attached to the head of the rock bolt, and the outer conductor of the coaxial cable is grounded to earth.

The generated electromagnetic wave propagates along the inner conductor of the coaxial cable and is transmitted to the rock bolt. The electromagnetic wave is reflected at the end of the bolt, received using the TDR, and recorded using a laptop computer with the waveform display software.

Finally, the length of the rock bolt is evaluated by estimating the difference in the time domain (Δt) between t_1 (the reflection from the head of the bolt) and t_2 (the reflection from the end of the bolt). The time difference between the initial and final inflection points of the signal is the round-trip travel time. The initial and final inflection points are determined as follows:

- The initial inflection point is determined as the intersection between the horizontal tangent line and the tangent line, with a negative slope at the local maximum value.
- The final inflection point is determined as the intersection between the horizontal tangent line and the tangent line, with a positive slope at the local minimum value (see Figure 33).

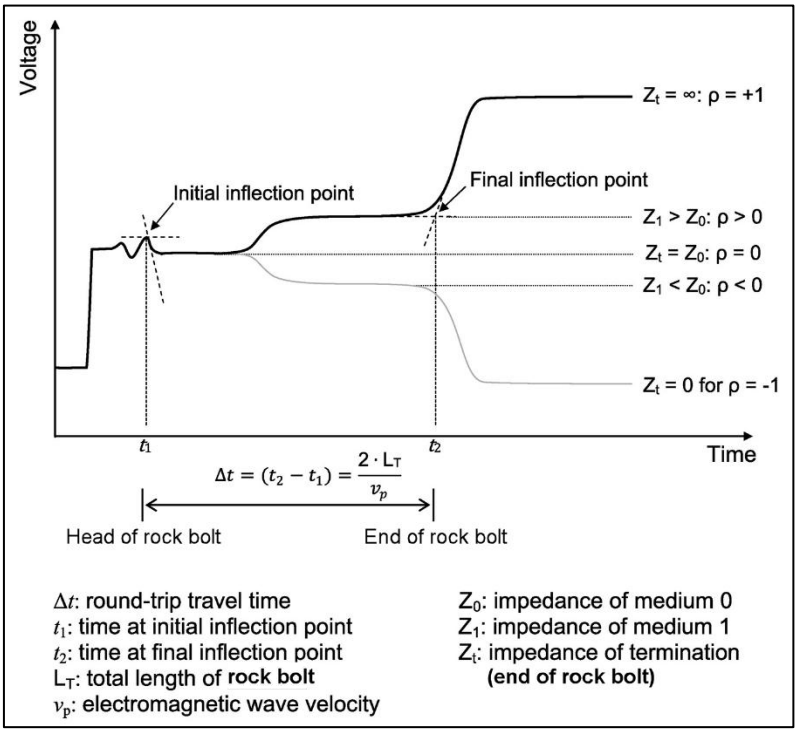

Figure 33. Typical TDR signal in soil nail and travel-time estimation [29].

Yu and Lee[30] conducted an experiment to evaluate the effectiveness of the electromagnetic waves to inspect defects in rock bolts. The study involved the analysis of nine rock bolt specimens: (i) one bolt was fully grouted and (ii) eight bolts were defective. Among the defective bolts, five had non-grouted sections at the ends with varying non-grouted ratios, and three contained different types of voids as illustrated in Figure 34. Rock bolt specimens were prepared in two different conditions, namely non-embedded and embedded in concrete block. The non-embedded condition indicates that rock bolts are only surrounded by cement grout. The embedded condition indicates that rock bolts are embedded in the concrete block, as shown in Figure 35, to simulate rock bolts installed in rock mass.

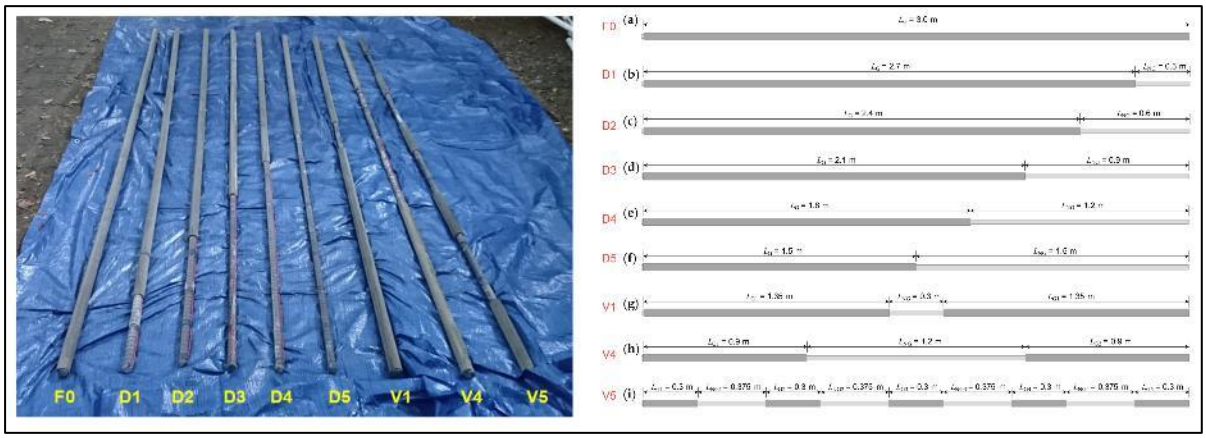

Figure 34. Rock bolt specimens for experiments [30].

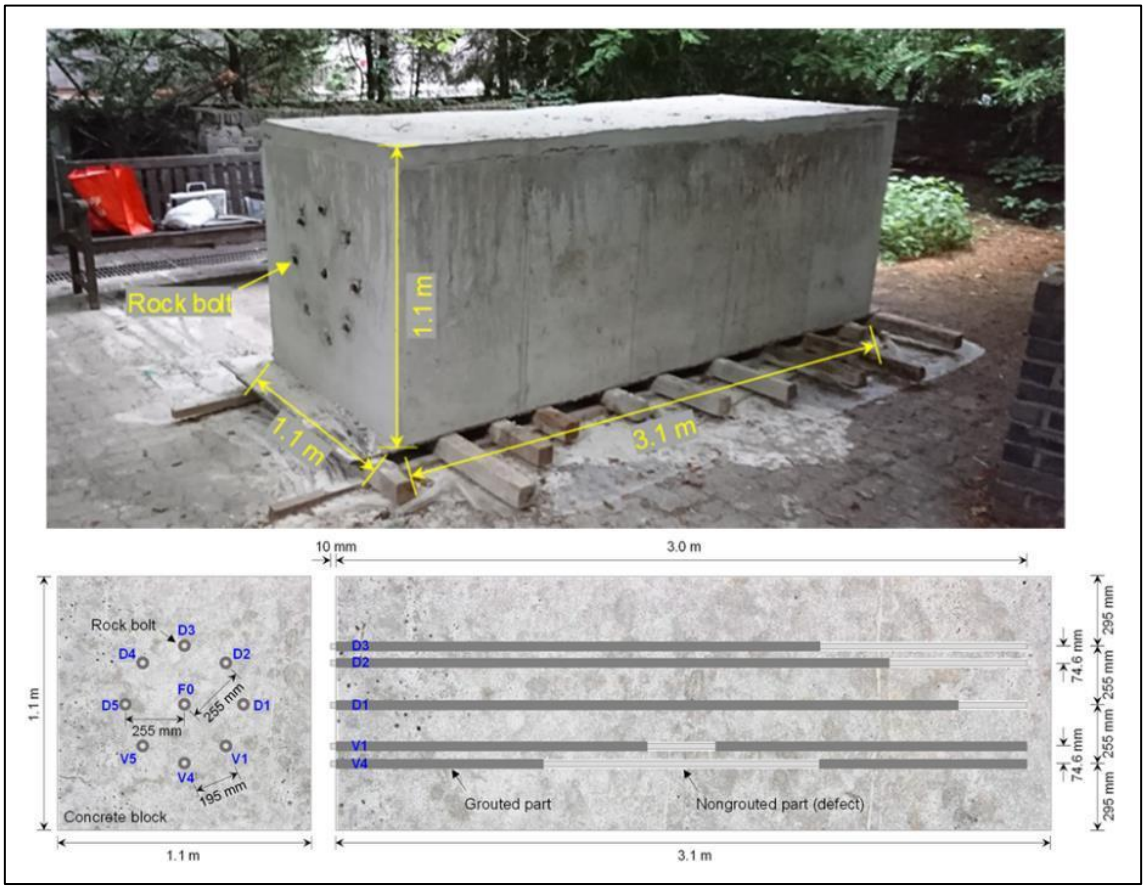

Figure 35. Concrete block with installed rock bolts for simulation of rock mass [30].

As presented in Figure 36, an initial inflection point was determined as the intersection between the horizontal and negatively sloped tangent lines at the trace's local maximum. The n^{th} inflection point, caused by a defect, was determined by locating the intersection between the horizontally flat and positively sloped tangent lines at the trace's local minimum. The final inflection point was determined by locating the intersection between two positively sloped tangent lines at the trace's local minimum. If a signal reflected at the end appears as a horizontally flat and a sloped line, the final inflection point was determined.

The round-trip travel time of electromagnetic waves reflected from the end of the rock bolt was calculated based on the time difference (Δt_{end}) between t_0 (time at the initial inflection point) and t_{end} (time at the final inflection point). The round-trip travel time of electromagnetic waves reflected from defects was determined by the time difference (Δt_n) between t_0 and t_n (time at the nth inflection point). The velocity of electromagnetic waves (v_p) in the rock bolt was calculated by the ratio of twice the length of the rock bolt to the travel time (Δt_{end}).

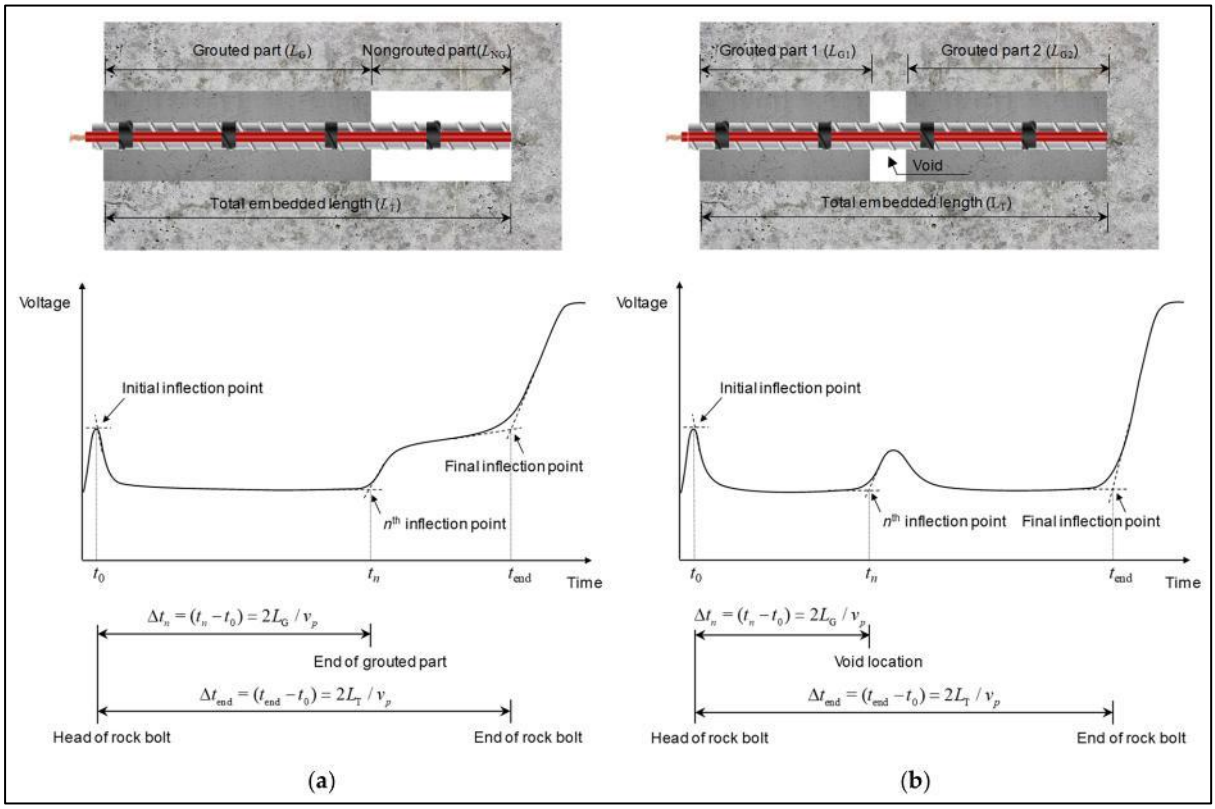

Figure 36. Waveforms of electromagnetic waves in defective rock bolts with: (a) non-grouted part at the end and (b) air void [30]. The RED wire is the grounded outer conductor.

The measured signals for rock bolts in the embedded condition are plotted in Figure 37. The reflections of electromagnetic waves at the heads, ends, and at defects are clearly detected, even though rock bolts are embedded in the concrete block. The round-trip travel times (t_0) of electromagnetic waves reflected at the heads of all rock bolts in the embedded condition are measured to be 0.88 ns [30].

- For the fully grouted rock bolt (F_0) in embedded condition, the electromagnetic waves are reflected at the head and end, as shown in Figure 37(a). The amplitude of the signal is attenuated in the grouted part and increases at the end. The time difference (Δt_{end}) between round-trip travel times of electromagnetic waves reflected at the head and end of the fully grouted rock bolt is measured as 53.75 ns.
- For the defective rock bolts D2, D3, D4, and D5 with non-grouted parts at their ends in the embedded condition, the reflections of electromagnetic waves appear at the defects (i.e., interfaces between grouted and non-grouted parts) as well as at the heads and ends, as shown in Figure 37(c–f), respectively.
- In the case of the defective rock bolt D1, however, no reflection at the defect is observed, as reflections at the defect and the end overlap each other. For the defective rock bolts D2, D3, D4, and D5, the respective time differences (Δt_1) between round-trip travel times of electromagnetic waves reflected at the interface between grouted and non-grouted parts (i.e., defects) are 41.58, 36.10, 32.15, and 26.00 ns, respectively. The time differences (Δt_{end}) between round-trip travel times

of electromagnetic waves reflected at the heads and ends are 51.04, 48.63, 45.81, 43.97, and 42.42 ns for D1, D2, D3, D4, and D5, respectively.

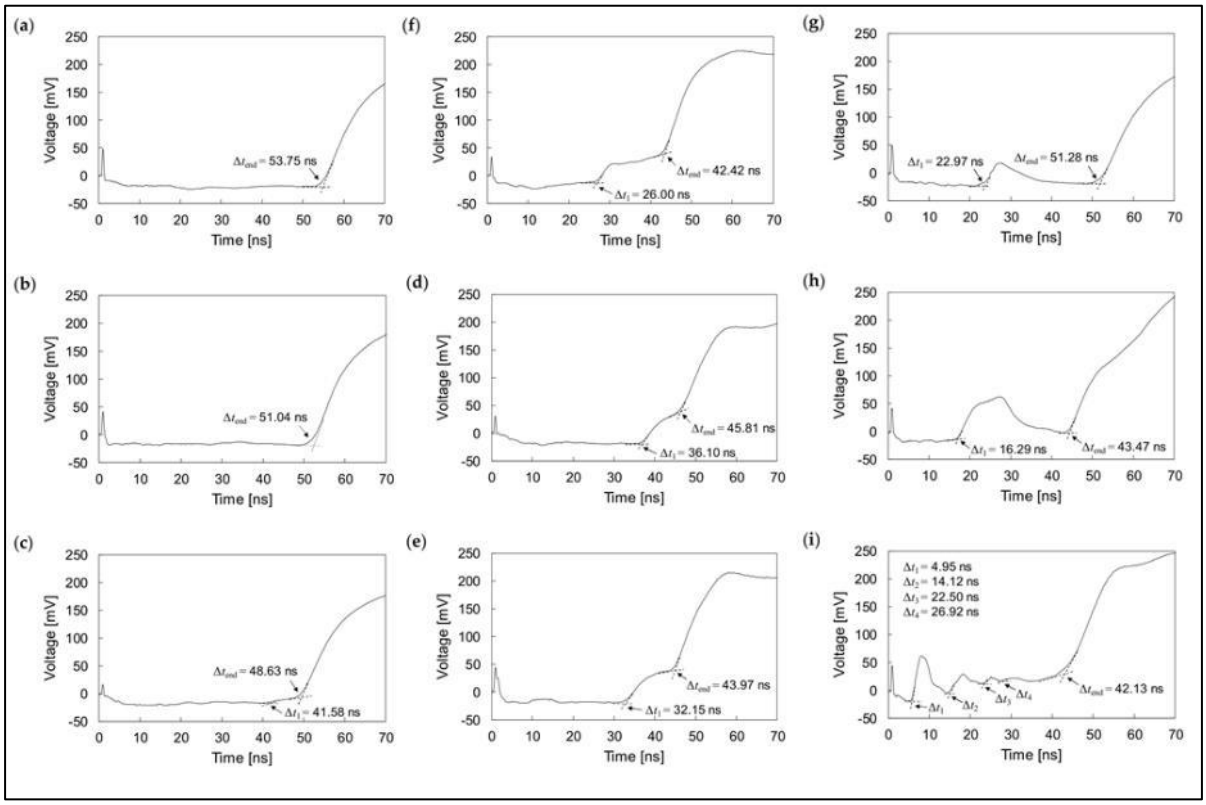

Figure 37. Measured signals in embedded condition for rock bolts presented in Figure 34 [30].

- The presence of voids in defective rock bolts in the embedded condition is clearly detected. The electromagnetic waves are observed to be reflected at voids, heads and ends of the defective rock bolts, as shown in Figure 37g–i. The signal amplitudes increase in the voids, whereas they decrease in the grouted parts. For the defective rock bolt V1, with one void in the middle, the difference in the round-trip travel time (Δt_1) between electromagnetic waves reflected at the head and the void is 22.97 ns, as shown in Figure 37g. For the defective rock bolt V4, the Δt_1 is measured to be 16.29 ns. The width of the reflected signal for V4 is larger than that for V1, as V4 has a larger void compared to V1. For the defective rock bolt V5, where four voids are present, four reflections by voids appear in the measured signal, as shown in Figure 37i. The Δt1, Δt2, Δt3, and Δt4 for the first, second, third, and fourth reflections are measured to be 4.95, 14.12, 22.50, and 26.92 ns, respectively. The differences in the round-trip travel times (Δt_{end}) between electromagnetic waves reflected at the heads and ends for the V1, V4, and V5 are 51.28, 43.47, and 42.13 ns, respectively.

3.5 Impact - echo test method

Impact-echo (IE) is a non-destructive, **acoustic method** that has been used in civil engineering since the mid-1980s. Currently, it is used in solid masonry construction for building component thickness measurement and locating structural elements and flaws. As in ultrasonic detection, (multiple) reflections of waves caused by impact-echo with a short-duration mechanical impact at material margins are measured. It is technically a relatively simple method that requires, as with almost all types of non-destructive material testing, some expertise in analysing the measurement results.

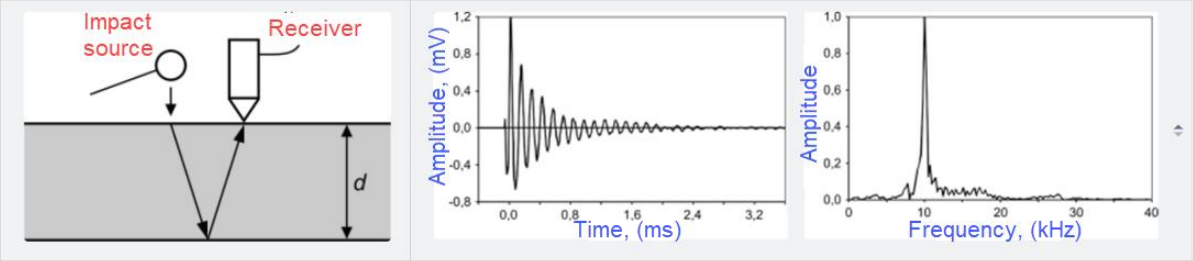

Figure 38. Time signal and frequency spectrum of an impact-echo measurement.

The Impact-Echo (IE) method uses stress waves to interrogate and evaluate both the length as well as the health of the rock bolt grouts. Similar to ultrasonic and electromagnetic techniques, the energy generated by the impactor travels through the material as stress waves and is reflected and scattered when they encounter an interface of sufficiently different impedance. If the dynamic load is applied to the rock bolt, particles within the rock bolt show compressive and dilative behaviour in the longitudinal direction which is also called P waves, and the propagation of such waves can be detected and recorded.

According to the National Cooperative Highway Research Program [31], the impact-echo method can be used to detect multiple types of flaws in rock bolt-type structures, including rock bolt length inadequacies or fractures, reduced cross-section area caused by corrosion, and the formation of cracks between rock bolts and the anchoring medium, or grout, due to poor contact.

Measurements and testing equipment

he impact echo test, as shown in Figure 39, may be used to evaluate cracking of grouts, fracture of tendons, and loss of element section. The specimen is impacted using a hammer or ball device, which generates elastic compression waves (P-Waves) with relatively low-frequency content. The traveling waves are reflected whenever a change in material or geometry is encountered along the length of the element. Equipment required for the impact echo test method includes an impact device, an accelerometer, velocity or displacement transducer for measuring the specimen response, and a data acquisition system. The signal is processed with a signal conditioner that also includes a power supply with necessary excitation. As shown in Figure 39, tests may be conducted with the impact and receiver placed at the same end of the bar [31].

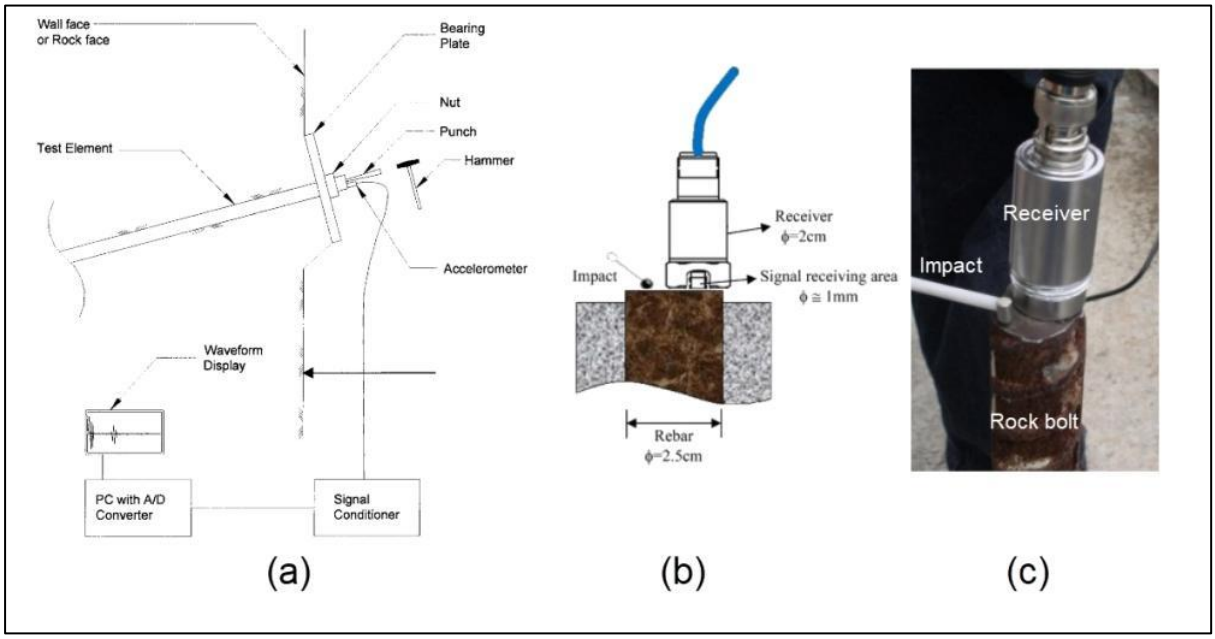

Figure 39.(a) Schematic of impact echo test, (b) configuration diagram of the Impact-echo experiment (c) the test instrument installation[31], [32].

Stress wave theory

When a transient impact load is applied to the top end (free end) of a rock bolt, the particles within the rock bolt member generate dilations and compressions in the longitudinal direction (P-waves), and these stress waves propagate forwards in a steady manner. When the stress waves encounter variable impedance interfaces, reflection and transmission take place, as shown in Figure 40.

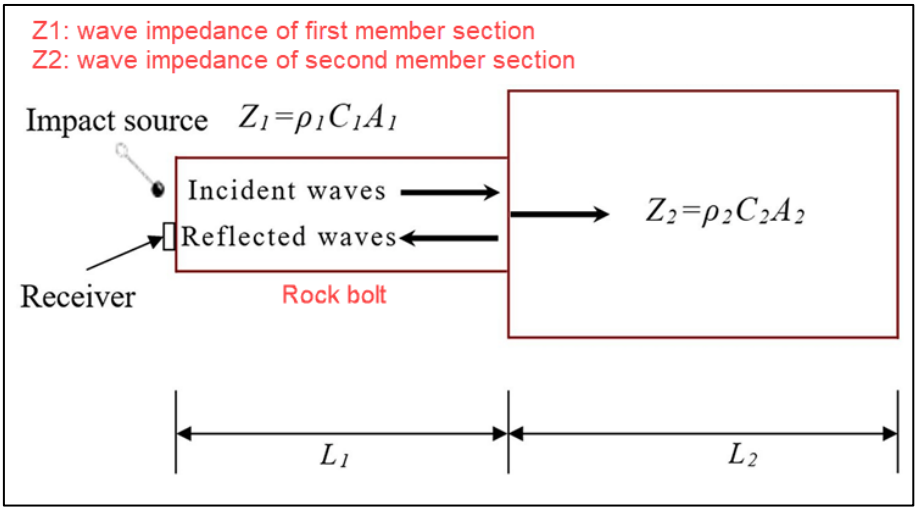

Figure 40. Reflection and transmission of stress waves at anchoring interface.

In impact-echo testing, impedance refers to a material's resistance to the propagation of stress waves. It's a key factor in how stress waves, generated by a mechanical impact, behaves within a material and are reflected at interfaces or flaws. Specifically, the acoustic impedance of a material is defined as the product of its density and the speed of sound within it. This impedance influences the reflection and transmission of stress waves at boundaries, making it a crucial parameter in analyzing the results of impact-echo tests. The wave impedance is calculated as follows:

$$Z = \rho * C * A \tag{8}$$

where ρ denotes the density of the medium, C is the velocity of the stress waves, and A represents the cross-section area of the medium [37].

Upon impact, the generated P-waves travel between the top and bottom of the rock bolt, producing periodic responses. The travel path of a P-wave for a single roundtrip is twice the depth of the defect (d). The resulting periodic wave corresponds to the path length of $2d$, divided by the apparent wave velocity $C_{P,apparent}$ of the rock bolt. The fundamental equation of impact-echo is:

$$d = \frac{C_{P,apparent}}{2f} \tag{9}$$

where d is the depth from which the stress waves are reflected (the depth of a flaw or the thickness of a solid structure), C is the apparent wave velocity, and f is the dominant frequency of the signal. The frequency f is obtained from the results of a test. To determine thickness or depth of a flaw, the wave speed $C_{P,apparent}$ must be known. Empirical compression wave velocity ≈ 5,5 km/s for steel could be used [36].

Once a digital displacement waveform is recorded, a Fast Fourier Transform (FFT) can be used to obtain the amplitude spectrum, see Figure 41,. This technique is based on the fact that any waveform can be represented by the sum of a series of sine waves of different amplitudes, frequencies, and phase angles. If the apparent wave velocity of a P-wave is known, then the rock bolt length or the depth of the defect can be obtained using the dominant frequency of the waveform.

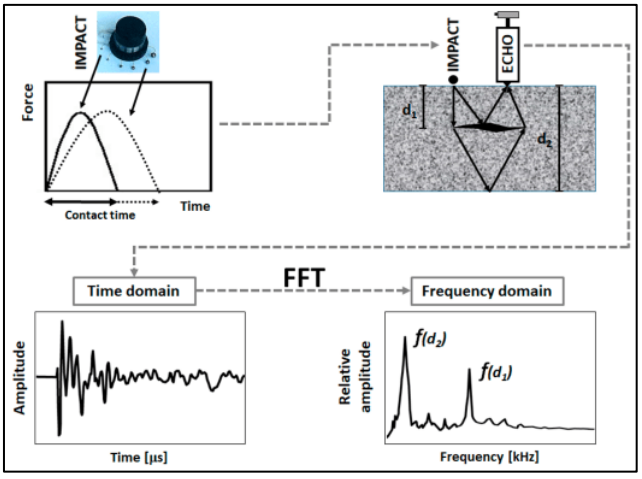

Figure 41. Schematic Diagram of Impact-Echo Method [33].

The example below illustrates the use of impact echo testing to study rock bolts measuring three-meter-long rock bolts at the State University of New York at Buffalo (UB) in 1999 [31]. In this setup, eight rebar, were installed as shown in Figure 42. These bars were arranged in two rows, with a separation of approximately 4.5 meters between the rows.

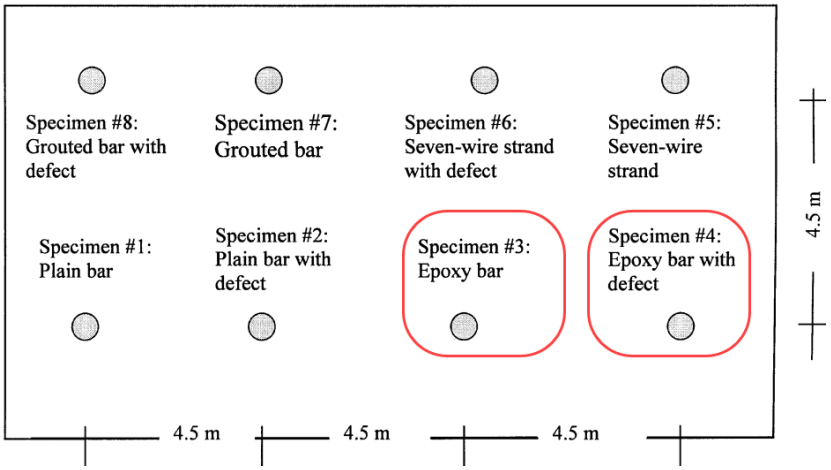

Figure 42. Plan view of in situ specimens at UB test facility.

Figure 43 and Figure 44 present the results from impact tests performed on epoxy-coated bars, with and without defects (elements 3 and 4). Reflections at intervals of approximately 0.0011 s are observed in the time domain. These reflections correspond to the time for compression waves to travel the length of the bar and back (2 × 3 m ÷ 5,500 m/s = 0.0011 s). For the bar with the defect, an additional reflection appears that becomes more apparent as energy from reflections at the end of the bar attenuate. The presence of a defect along the length of the bar is also characterized in the frequency response presented in Figure 44. Compared with the intact specimen, the lower fundamental frequencies are relatively more predominant in the frequency response of the defected bar. Table 2 is a summary of the frequencies observed in the impact test results for each of the elements at the UB test location.

Table 2. Summary of the frequencies observed in the impact testing for the tested bars [31].

Element #	Description	Frequency (Hz)						
		f_1	f_2	f_3	f_4	f_5	f_6	f_7
3	Epoxy-coated bar (d = 32 mm)	732	1465	2295	3125	3955	4834	5615
4	Epoxy-coated bar with defect (d = 32 mm)	684	1465	2246	3125	4004	4785	-

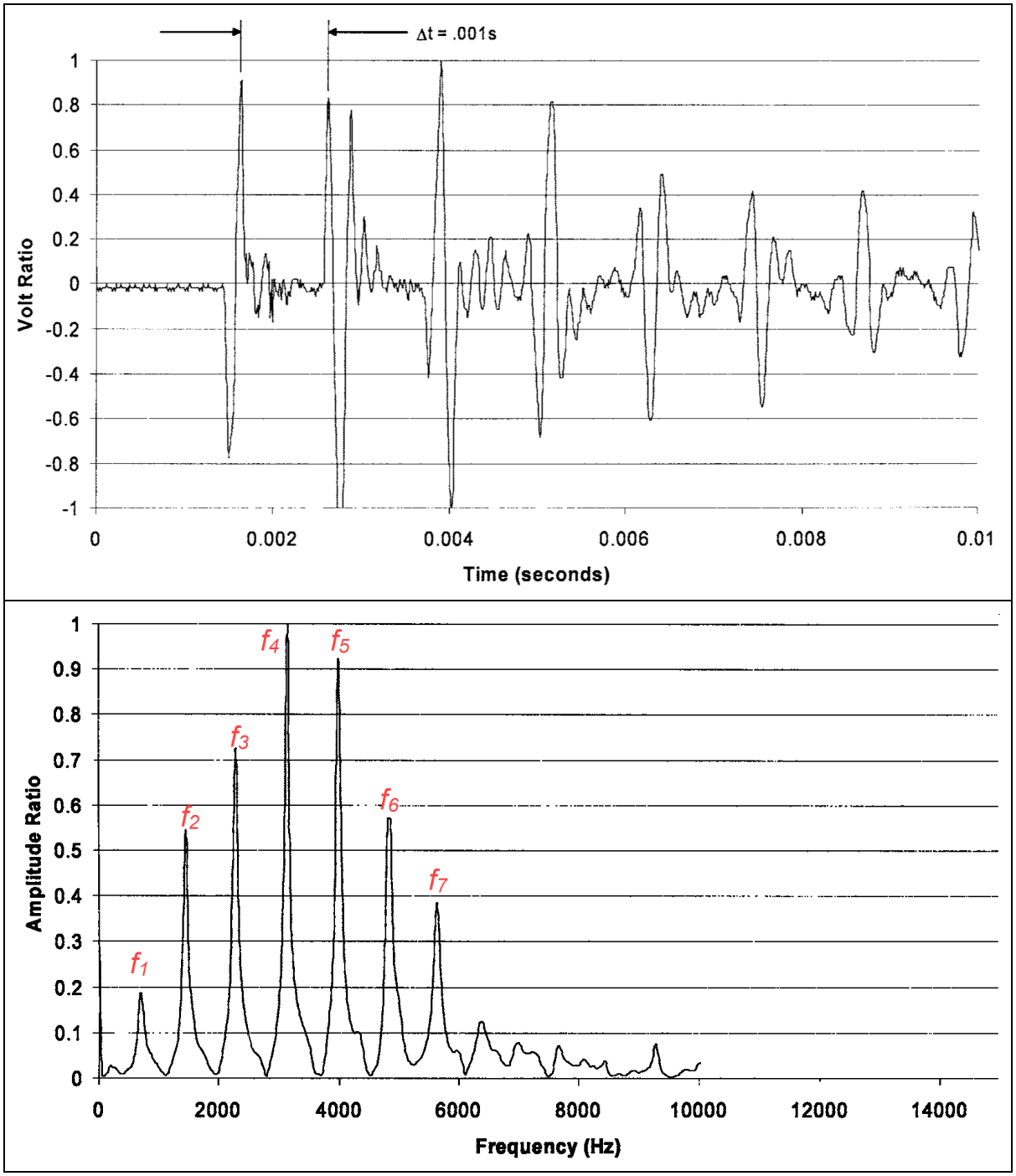

Figure 43. Time domain and amplitude spectrum from impact test on epoxy-coated bar without defect at UB test facility [31].

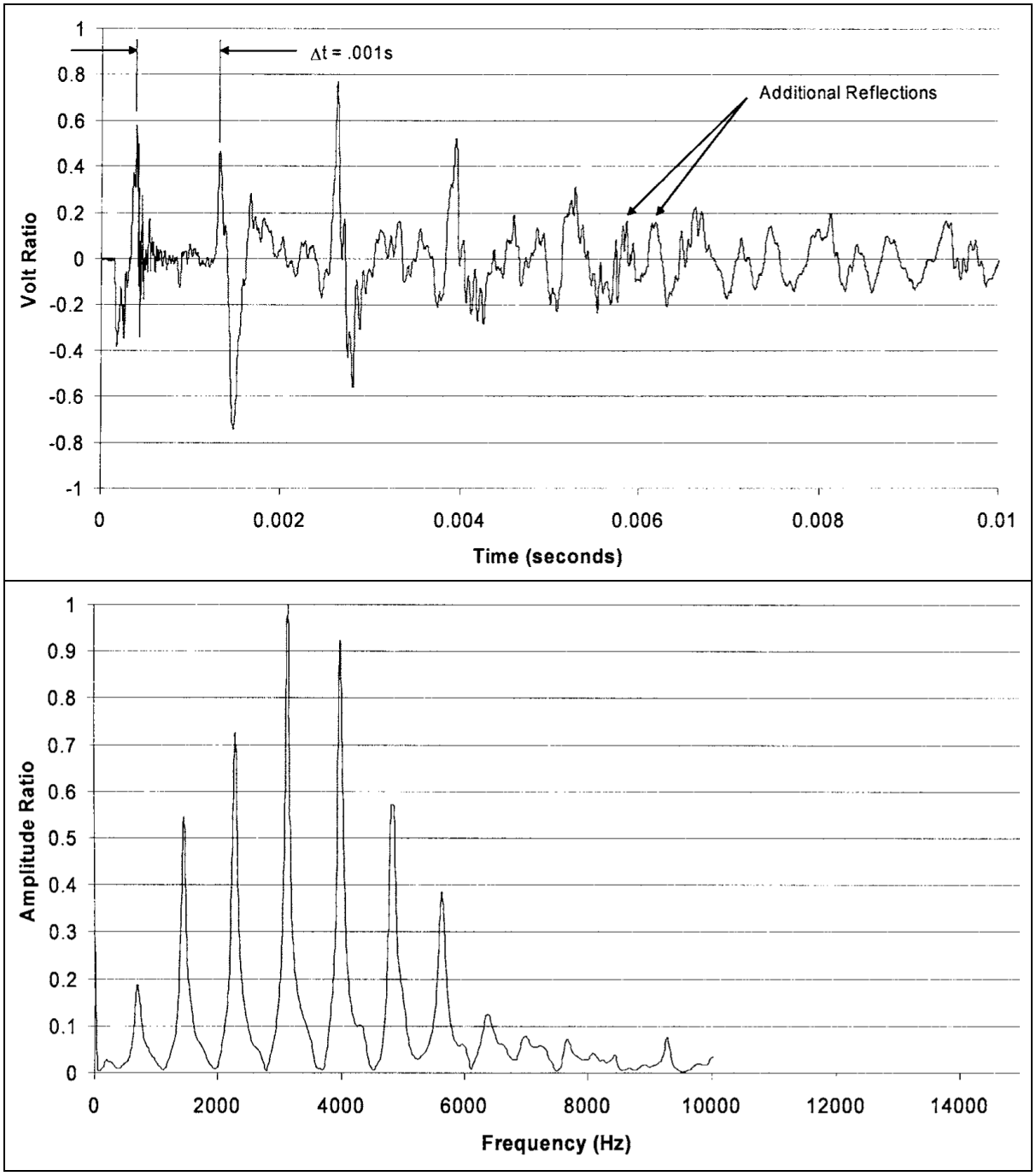

Figure 44. Time domain and amplitude spectrum from impact test on epoxy-coated bar with defect.

3.6 Smart sensors — Fiber Optic Sensors

Fiber optic sensors are a category of sensors that use the optical fiber or the light traveling through the fiber as the sensing element. Properties of the light will change due to external perturbations such as strain, pressure, temperature and electric currents experienced by the fiber optic. An optical fiber sensor system typically consists of a light source, a receiver, an optical fiber as the sensing element, a modulator, and a signal processing unit. The fiber optic sensors convert or encode these external perturbations into corresponding variations in the optical properties of the transmitted light, such as intensity, phase, wavelength, frequency and polarization [34]. Such variations are then demodulated by a dedicated demodulation system.

Fiber optic sensors have several distinctive advantages over conventional electrical sensors which include small size, high sensitivity, corrosion resistance, immunity to electromagnetic interference, and ability to multiplex. Therefore, fiber optic sensors have been widely used in monitoring various engineering structures. Among the various types of fiber optic sensors, (i) the Fiber Bragg Grating (FBG) sensors and (ii) Brillouin Optical Time Domain Reflectometer (BOTDR) sensors have shown the most promise in the field of structural health monitoring [35].

3.6.1 Fiber Bragg Grating (FBG) Sensors

A FBG is produced by inscribing periodic and permanent modifications in the core refractive index along the optical fiber axis [36]. When a broadband light is launched through the gratings, the reflected Bragg wavelength follows the form:

$$\lambda_B = 2 * n_{eff} * \Lambda \tag{10}$$

where λ_B is the Bragg wavelength, n_{eff} is the effective refractive index of FBG and Λ is the grating period.

The grating period, and therefore the Bragg wavelength, are linear to both strain and temperature. The relation between the relative Bragg wavelength shift and the axial strain ε and the temperature variation ΔT is expressed as follow:

$$\frac{\Delta\lambda_B}{\lambda_B} = C_\varepsilon * \varepsilon + C_T * \Delta T \tag{11}$$

where C_ε and C_T are strain and temperature sensitivity coefficients, respectively.

As illustrated in Figure 45, when a broadband light passes through optical fiber grating, the portion of the spectrum which equals to the Bragg wavelength of the FBG is reflected, and others can pass through the FBG with small attenuation. In this way, the interrogation of FBG sensors can be easily multiplexed using the Wavelength Division Multiplexed (WDM) technique to realize a quasi-distribution sensor network [37].

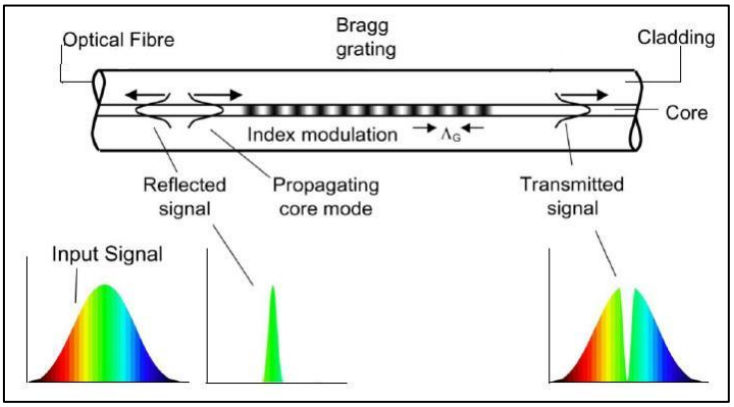

Figure 45. Functioning principle of the FBG sensor.

3.6.2 Brillouin Optical Time Domain Reflectometer (BOTDR) Sensors

Brillouin scattering is a phenomenon in which a light wave transmitted in an optical fiber is scattered by the interaction with acoustic waves. The frequency of the scattered Brillouin light is dependent on the strain and temperature of the optical fiber, which will shift from the frequency of the incident light. The Brillouin frequency shift v_B is given by the following equation:

$$v_B = \frac{2n * v_A}{\lambda} \tag{12}$$

where n is the refractive index, v_A is the sound wave velocity and λ is the wavelength of incident light.

The Brillouin frequency shift is linearly proportional to the change of strain or temperature, which is expressed as follows:

$$v_B(\varepsilon, T) = v_{B0}(\varepsilon_0, T_0) + C_\varepsilon(\varepsilon - \varepsilon_0) + C_T(T - T_0) \tag{13}$$

where $v_B(\varepsilon, T)$ is the Brillouin frequency shift at strain ε and temperature T; C_ε and C_T are the strain and temperature coefficients, respectively; T_0 and ε_0 are the initial strain and initial temperature that correspond to the reference Brillouin frequency v_{B0}.

Figure 46 (a) shows the Brillouin scattering intensity distribution at different frequencies along the optical fiber. Figure 46(b) shows the frequency shift of the Brillouin back scattering light at a specific location due to its corresponding strain, Figure 46(c) shows the Brillouin scattering intensity spectrum at a specific frequency along the optical fiber. BOTDR is very suitable for long-distance distributed strain sensing with a sensitivity of 5 με [38]. Howevetherefore,,atial resolution is relatively low, about 1 m, and therefore this technique is not suitable for structural monitoring applications that require dense distribution of sensors.

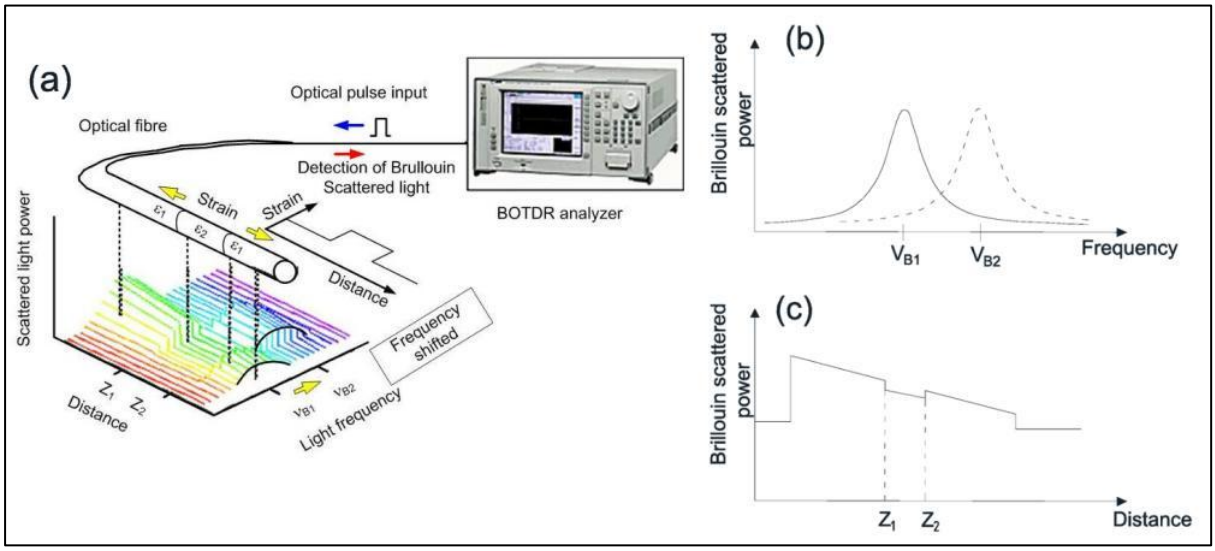

Figure 46. Principle of the Brillouin Scattering-based fiber optic measuring technique: (a) The Brillouin scattering spectrum along an optical fiber; (b) The Brillouin scattering spectrum at a specific frequency; (c) The Brillouin scattering spectrum at a specific location[3].

3.6.3 Corrosion Monitoring using smart sensors

Considering that extensive corrosion products can exert expansive stress on the surrounding rock mass, Wei et al. [40] proposed an early-stage method for monitoring rock bolt corrosion (Accelerated Corrosion Tests) by measuring the corrosion-induced strain with a fiber-optic Michelson interferometer, as presented in Figure 47.

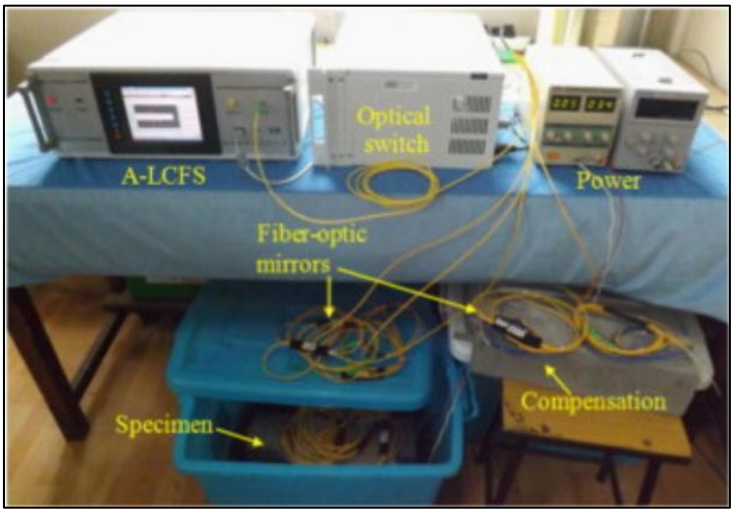

Figure 47. The setup for electrochemical corrosion acceleration experiment [35].

Two methods of twisting optical fiber onto the rock bolt were tested: (i) one involved directly winding the fiber around the bolt, and (ii) the other used a mortar cushion placed between the fiber and the bolt, as presented in Figure 48(a and b). The latter method exhibited more uniform strain development during accelerated corrosion tests, as illustrated in Figure 49. The results confirmed the effectiveness of this sensing technique for early detection of rock bolt corrosion.

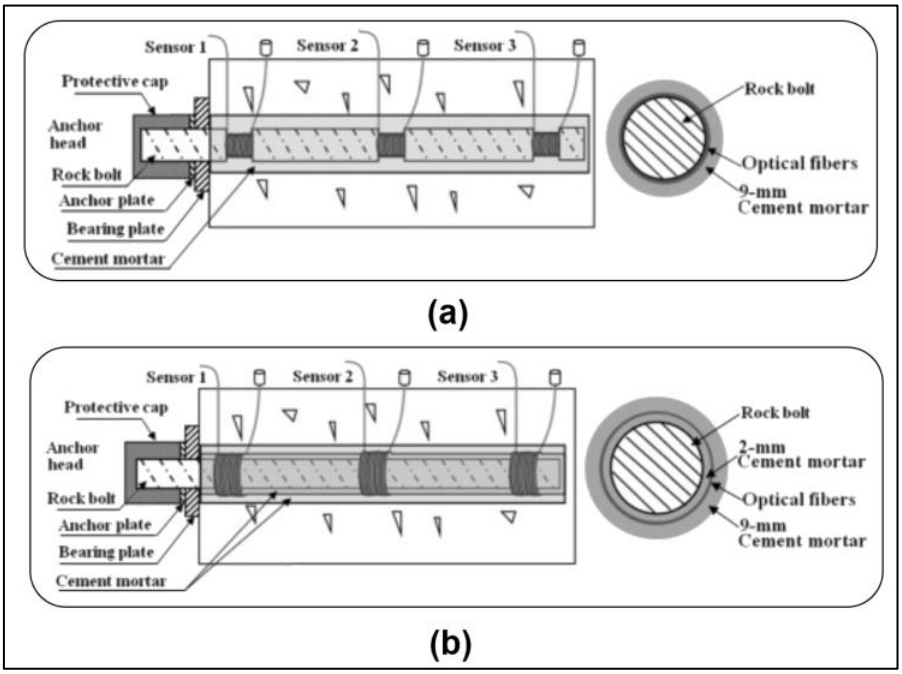

Figure 48. (a) The sensing fiber was twisted on the surface of steel rock bolt directly, formed a (Rock bolt)–(Optical fiber)–(Cement mortar) structure and represented as R–O–C and (b) Schematic of the corrosion expansion sensor with 2 mm cement mortar cushion, which formed a (Rock bolt)–(Cement mortar)–(Optical fiber)–(Cement mortar) structure and represented as R–C–O–C [35].

In Figure 48, the concrete specimen was put on a plastic support, and 1/5 of its volume emerged in the sea water. Whereas the horizontal position of rock bolt embedded in the specimen was above the solution. There was a stainless-steel plate at the bottom of the bath container. When the specimen was placed in the bath solution for one or two days, a 50 mA constant current was applied from the rock bolt through the bath solution to the plate that the rock bolt acted as an anode and the plate functioned as a cathode. During the experiments, the specimen with reference fiber was put in the same environment in order to get a reference of environmental influence.

The results measured by the three sensors can be modelled by this three-stage process.

I. After applying constant electrical current, the results from sensor 1 was keep on silence in the first 100 h, which can be treated as the initiation stage.
II. From the time 100 to 432 h, the average strain measured increased continuously from zero to 2670 με, which can be named as the activation stage and indicated as II.
III. From 432 h to 480 h, the strain was slowly increased and presented as a deterioration stage III.

When corrosion happens, the volume of the corrosion stuffs was bigger than the corresponding steel, leaded to an expansion and thereby stretched the sensing fibers. Figure 49(a and b) showed the results how the sensing fiber in the R–O–C configuration to response the expansion in the 30 days experiment. The results from sensor 1–3 demonstrated that they suffered from the fluctuation of temperature in 24-h periodicity with amplitude of about 300 με. To eliminate these fluctuations, we introduced the temperature compensation by using a reference fiber.

- The results from sensor 1 had a sharp increase in its measured strain, while the other two had a moderated increasing speed, especially within the 550 h of the acceleration corrosion experiments. However, the results from the sensor 1 had reached about 2670 με at 432 h after beginning the experiment. While the maximum strain of 1070 με at 552 h from sensor 2 and 1410 με at 608 h from sensor 3 were observed. This large difference in strains measured by the three sensors demonstrated that the corrosion was non-uniformly developed inside the concrete when the sensing fiber being configured as the R–O–C model showed in Figure 48(a).
- Figure 49(c) presents the results from the sensors without any compensations on temperatures. Figure 49(d) shows the results of three sensors after compensating the influence of temperature. We can find that the results from all the three sensors have no obvious difference during the first stage, showed as I, a 436-h accelerated corrosion experiment. The tendencies of the three sensors appeared a slightly difference in the time between 436 and 568 h and the maximum strains were 3362 με, 2975 με and 2846 με corresponding to sensor 1–3, respectively, in the stage II. And finally, the three strains showed a rundown to 350 με, 210 με and 100 με, respectively. It was different with the results obtained in R–O–C sensors.

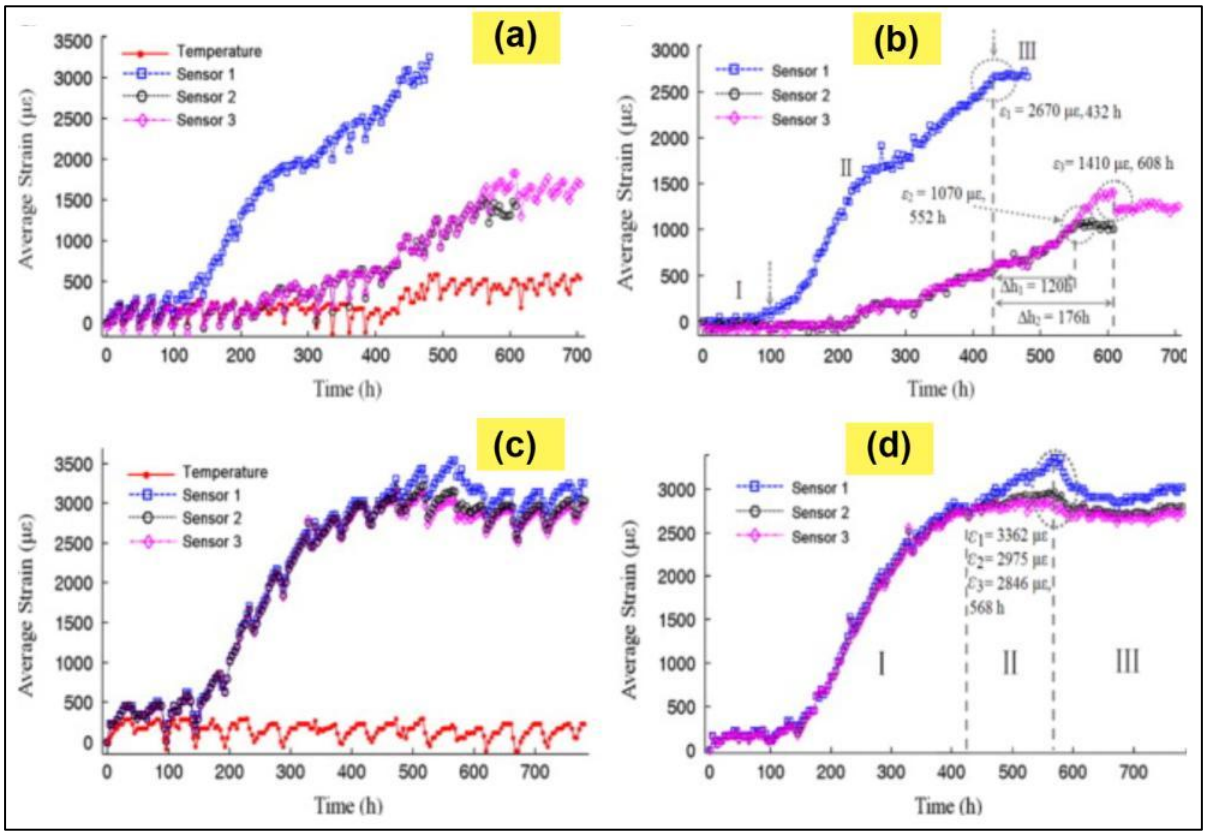

Figure 49. The results of R–O–C configuration. (a) The uncompensated results without the reference fiber. (b) The results after compensated by the reference sensing fiber. The results from the sensor in R–C–O–C configuration. (c) The uncompensated results without the reference fiber. (d) The results after compensated by the reference sensing fiber [35].

After the experiment was done, some cracks were found on the surface of specimens as shown in Figure 50.

- Figure 50(a) showed that the specimen with sensors in R–O–C configuration had a large crack with a maximum width of 1.5 mm at the lateral and the specimen with sensors in R–C–O–C configuration had a large crack with a maximum width of 0.9 mm at the bottom. There were rust products spilled out on the surface of specimens.
- Figure 50(b) showed that crack happened at the part of anchor head and the maximum crack widths were 1.3 mm and 1.1 mm separately.
- Figure 50(c) showed that the rock bolts corroded after experiments.

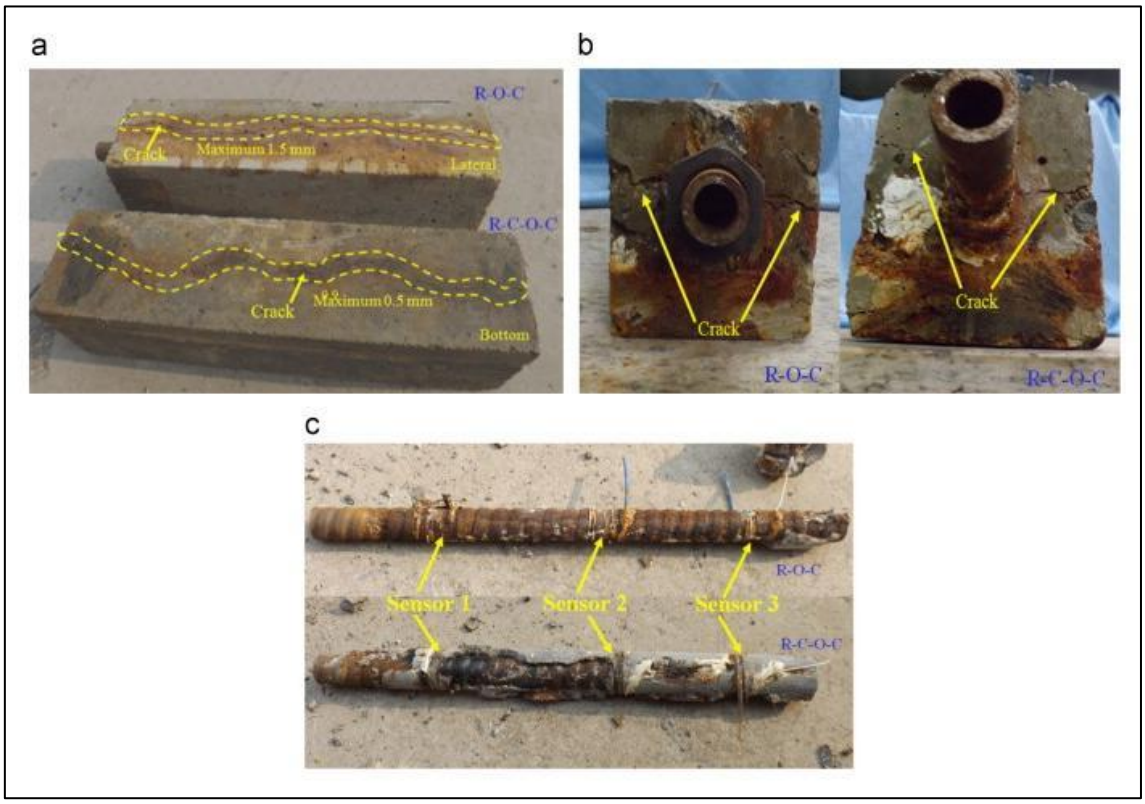

Figure 50. The samples after accelerated corrosion experiments. (a) Cracks found outside of the specimen. (b) Crack found near anchor head. (c) Rock bolts corroded after experiments.

4 Summary and conclusions

Since rock bolts are usually embedded in concrete or grouted into rock, visually inspecting them for corrosion is challenging. Non-destructive testing (NDT) methods are invaluable for assessing the internal condition of these bolts without causing damage. Detecting corrosion is crucial for maintaining structural integrity, especially in underground environments. As visual inspections may not accurately reveal the true condition of rock bolts, NDT methods are essential. Techniques such as electrochemical potential measurements, ultrasonic guided wave technology, electromagnetic wave methods, and fiber optic sensors offer promising solutions for detecting corrosion and monitoring changes in bolt conditions.

In this state-of-the-art report, the common types of rock bolts use in tunnel walls strengthening and the corrosion process of these rock bolts are briefly reviewed, followed by a description of the state-of-the-art applications of the commonly used non-destructive testing (NDT) methods used in rock bolts condition monitoring. The report discusses the measurement principles, instruments, and examples of results analysis for various NDT methods, evaluating their effectiveness in detecting corrosion in rock bolts.

1) **Electrochemical Open Circuit Potential (OCP)**: This in-situ method determines corrosion potential and is considered useful for assessing corrosion risk. OCP values are higher under wet surface conditions compared to those on dry surfaces, indicating that higher OCP values (expressed in negative millivolts) correspond to increased corrosion potential. Surfaces with relative humidity above 60% create favourable conditions for corrosion, requiring careful analysis of OCP readings in such environments. For consistency, OCP measurements of rock bolts, from the bolt head to the reference electrode placement, are standardized to be less than 30 cm. Although OCP does not account for other significant factors, such as induced stress in the bolt, it is quick to perform and serves as a valuable initial assessment tool.
2) **Ultrasonic pulse-echo:** Ultrasonic pulse echo measurements provide a quantitative assessment of the energy of echoes from the walls and ends of rock bolts. When rock bolts experience corrosion, there is a noticeable decrease in echo energy, whereas the energy of the echoes remains unchanged if corrosion is absent. The ultrasonic pulse-echo technique measures the energy of reflected ultrasonic waves, with a reduction in energy signalling corrosion-induced flaws.
3) **Ultrasonic Guided Wave Technology:** This method utilizes elastic waves to detect changes in bolt properties caused by corrosion. Guided waves are particularly sensitive to corrosion, enabling the monitoring of interface changes at specific frequencies. The technique involves transmitting a signal through the bolt and analyzing the reflected or scattered waves to identify corrosion-related alterations. Instruments such as the Rock Bolt Tester and Boltometer employ ultrasonic guided wave technology to monitor the condition of rock bolts and grout. The application of guided ultrasonic waves for in-situ identification of rock bolt condition shows promises as an effective testing method.

4) **Electromagnetic waves method**: Electromagnetic waves (generated and detected by Time Domain Reflector, TDR) can be used to detect corrosion and other defects in rock bolts, which are critical for ground support in underground excavations and slopes. This technique operates on the principle that electromagnetic waves propagate differently through materials with distinct dielectric constants, such as steel, grout, and air. By analyzing reflections and alterations in the electromagnetic wave patterns, it is possible to point the location and extent of corrosion or other defects.
5) **Impact - echo test method**: The impact-echo method is an effective non-destructive testing technique for detecting corrosion in rock bolts. It helps identify flaws such as reduced cross-sectional areas due to corrosion, inadequate embedment length, and fractures or cracks between the bolt and surrounding material. By analyzing the reflections of ultrasonic waves transmitted through the bolt, this method provides an assessment of its condition.
6) **Smart sensors — Fiber Optic Sensors:** Over the past decades, fiber optic sensor techniques have transitioned from experimental stages to practical applications. These sensors can be embedded within the rock bolt structure to monitor strain and other parameters associated with corrosion. Offering high sensitivity, fiber optic sensing enables the tracking of corrosion-induced expansion, providing valuable insights into the bolt's condition over time.

One of the primary challenges in detecting corrosion in installed rock bolts is their limited exposure. In the field, corrosion is difficult to identify and quantify because only a small segment of the bolt is accessible for measurement. Researchers have previously employed ultrasonic methods to investigate corrosion in rock bolts, and while these techniques successfully identify corrosion sites, prior research offers limited details regarding the types of monitoring systems and conditions under which the bolts have been tested.

Given the widespread use of rock bolts in engineering fields such as civil construction, tunnelling, and mining, they serve as essential tools for ensuring underground safety. Therefore, it is crucial to reliably assess the condition of installed rock bolts before they fail, as corrosion reduces tensile strength and load-bearing capacity. Weakened or damaged rock bolts pose a risk to underground structures, which could lead to catastrophic failures, resulting in financial losses and potential fatalities. As more advanced non-destructive testing (NDT) methods are developed, they can be used individually or in combination to provide a comprehensive evaluation of rock bolts' condition.

5 References

[1] B. Lama and M. Momayez, “Review of Non-Destructive Methods for Rock Bolts Condition Evaluation,” *Mining 2023, Vol. 3, Pages 106-120*, vol. 3, no. 1, pp. 106–120, Feb. 2023, doi: 10.3390/MINING3010007.

[2] A. Ma, “Rock Bolts vs. Rock Anchors: Understanding the Key Differences.” Accessed: Jan. 19, 2026. [Online]. Available: https://apexroc.com/blog/rock-bolts-vs-rock-anchors/

[3] G. Song, W. Li, B. Wang, and S. C. M. Ho, “A review of rock bolt monitoring using smart sensors,” 2017. doi: 10.3390/s17040776.

[4] D. Sigh, A. Mishra, and H. Agrawal, “Performance evaluation of fully grouted rock bolt in an Indian hard rock underground mine,” in *Indian Rock Conference (INDOROCK 2016)*, Mumbai, India: Indian Rock Conference (INDOROCK 2016), Jan. 2016. Accessed: Jan. 27, 2026. [Online]. Available: https://www.researchgate.net/publication/311708625_Performance_evaluation_of_fully_grouted_rock_bolt_in_an_Indian_hard_rock_underground_mine

[5] K. Peter *et al.*, “An Overview of the Use of Rockbolts as Support Tools in Mining Operations,” *Geotechnical and Geological Engineering*, vol. 40, no. 4, pp. 1637–1661, Apr. 2022, doi: 10.1007/S10706-021-02005-5.

[6] N. Aziz, P. Craig, J. Australia, J. Nemcik, F. I. Hai, and F. Hai, “Rock bolt corrosion - an experimental study,” Jan. 2013, Accessed: Jun. 24, 2025. [Online]. Available: /articles/conference_contribution/Rock_bolt_corrosion_-_an_experimental_study/27686397/1

[7] C. C. Li, *Rockbolting: Principles and applications*. 2017.

[8] C. J. Manquehual, P. D. Jakobsen, and A. Bruland, “Corrosion Level of Rock Bolts Exposed to Aggressive Environments in Nordic Road Tunnels,” *Rock Mech. Rock Eng.*, vol. 54, no. 11, pp. 5903–5920, Nov. 2021, doi: 10.1007/S00603-021-02547-3.

[9] J. M. Roy, R. Preston, and R. P. Bewick, “Classification of Aqueous Corrosion in Underground Mines,” *Rock Mech. Rock Eng.*, vol. 49, no. 8, pp. 3387–3391, Aug. 2016, doi: 10.1007/S00603-016-0926-Z/FIGURES/4.

[10] G. Han, S. Lv, Z. Tao, X. Sun, and B. Du, “Evaluation of Bolt Corrosion Degree Based on Non-Destructive Testing and Neural Network,” *Applied Sciences 2024, Vol. 14, Page 5069*, vol. 14, no. 12, p. 5069, Jun. 2024, doi: 10.3390/APP14125069.

[11] W. Feng, A. Tarakbay, S. Ali Memon, W. Tang, and H. Cui, “Methods of accelerating chloride-induced corrosion in steel-reinforced concrete: A comparative review,” *Constr. Build. Mater.*, vol. 289, p. 123165, Jun. 2021, doi: 10.1016/J.CONBUILDMAT.2021.123165.

[12] C. Ngamkhanong, T. Li, S. Keawsawasvong, W. Frenelus, H. Peng, and J. Zhang, “An Insight from Rock Bolts and Potential Factors Influencing Their Durability and the

Long-Term Stability of Deep Rock Tunnels," *Sustainability 2022, Vol. 14, Page 10943*, vol. 14, no. 17, p. 10943, Sep. 2022, doi: 10.3390/SU141710943.

[13] N. Aziz, P. Craig, J. Nemcik, and F. Hai, "Rock bolt corrosion - An experimental study," *Transactions of the Institutions of Mining and Metallurgy, Section A: Mining Technology*, vol. 123, no. 2, 2014, doi: 10.1179/1743286314Y.0000000060.

[14] M. Bačić, K. Gavin, and M. Saša Kovačević, "Trends in non-destructive testing of rock bolts," 2019. doi: 10.14256/JCE.2727.2019.

[15] A. Spearing, K. Mondal, G. Bylapudi, and J. Hirschi, "A Method to Determine the Corrosion Potential of Rock Bolts on Coal Mines," *29th International Conference on Ground Control in Mining*, vol. 29, 2010, Accessed: Jul. 29, 2025. [Online]. Available: https://www.researchgate.net/publication/273831798_A_Method_to_Determine_the_Corrosion_Potential_of_Rock_Bolts_on_Coal_Mines

[16] A. Spearing, G. Bylapudi, K. Mondal, and A. Bhagwat, "Rock anchor corrosion potential determination in US underground coal mines," *6th South African Rock Engineering Symposium SARES 2014*, 2014, doi: 10.1520/C0876-09.

[17] FPrimeC, "Ultrasonic Testing of Anchor Bolts." Accessed: Jun. 25, 2025. [Online]. Available: https://fprimec.com/ultrasonic-testing-of-anchor-bolts/

[18] A. Staniek, "Identification of rock bolt length in situ conditions," *Diagnostyka journal, Polish Society of Technical Diagnostics*, 2021, doi: 10.29354/diag/135850.

[19] R. Amundsen, "Non-Destructive Testing of Grouted Rock Bolts in the Devoll Hydropower Project," Trondheim, Dec. 2017. Accessed: Jun. 26, 2025. [Online]. Available: https://www.researchgate.net/publication/340378065_Non-Destructive-Testing_Report_sponsored_by_Statkraft

[20] P. Choquet, "Rock Bolting Practical Guide-Pierre Choquet-Laval", Accessed: Jul. 28, 2025. [Online]. Available: https://www.researchgate.net/publication/348559648

[21] A. Kelly and A. Jager, "Critically evaluate techniques for the in situ testing of steel tendon grouting effectiveness as a basis for reducing fall of ground injuries and fatalities," 1996. Accessed: Jul. 28, 2025. [Online]. Available: https://researchspace.csir.co.za/dspace/handle/10204/1693

[22] T. Väisänen, "Documentation and quality control in rock bolting," Saimaa University of Applied Sciences, Lappeenranta, Lappeenranta, 2010. Accessed: Jul. 28, 2025. [Online]. Available: https://www.theseus.fi/bitstream/handle/10024/27424/Vaisanen_Tapio.pdf

[23] R. Van Wyk, "Non-destructive impact-testing as a method for roof bolt integrity analysis," 2015. Accessed: Jul. 29, 2025. [Online]. Available: https://core.ac.uk/download/pdf/54188248.pdf

[24] Z. Sun *et al.*, "An Ultrasonic Rock Bolt Sensing Technology (I): Methodology and Laboratory Studies," *Rock Mech. Rock Eng.*, vol. 57, no. 9, pp. 7387–7406, Sep. 2024, doi: 10.1007/S00603-024-03921-7/FIGURES/37.

[25] T. Stepinski and K. J. Mattson, “Instrument for rock bolt inspection by means of ultrasound,” *2015 IEEE International Ultrasonics Symposium, IUS 2015*, Nov. 2015, doi: 10.1109/ULTSYM.2015.0343.

[26] S. Krekula, F. Lanaro, and T. Stepinski, “Development of the instrument RBT with respect to rock bolt types PC- and CT-bolt and similar combination bolts,” 2021, Accessed: Jul. 29, 2025. [Online]. Available: https://urn.kb.se/resolve?urn=urn:nbn:se:trafikverket:diva-17677

[27] T. Stepinski and K.-J. Matsson, “Rock Bolt Inspection by Means of RBT Instrument,” *19th World Conference on Non-Destructive Testing*, 2016.

[28] J. S. Lee and J. D. Yu, “Nondestructive evaluation of grout defect in rock bolt using electromagnetic waves,” *Developments in the Built Environment*, vol. 17, p. 100365, Mar. 2024, doi: 10.1016/J.DIBE.2024.100365.

[29] J. D. Yu, K. H. Kim, and J. S. Lee, “Nondestructive health monitoring of soil nails using electromagnetic waves,” *Canadian Geotechnical Journal*, vol. 55, no. 1, pp. 79–89, 2018, doi: 10.1139/CGJ-2017-0043/ASSET/IMAGES/LARGE/CGJ-2017-0043F12.JPEG.

[30] J. D. Yu and J. S. Lee, “Smart Sensing Using Electromagnetic Waves for Inspection of Defects in Rock Bolts,” *Sensors 2020, Vol. 20, Page 2821*, vol. 20, no. 10, p. 2821, May 2020, doi: 10.3390/S20102821.

[31] J. Withiam, K. Fishman, and M. Gaus, “Recommended Practice for Evaluation of Metal-Tensioned Systems in Geotechnical Applications,” American Public Transportation Association, Washington, 2002. Accessed: Jul. 31, 2025. [Online]. Available: https://onlinepubs.trb.org/onlinepubs/nchrp/nchrp_rpt_477.pdf

[32] Y. F. Lin, J. W. Ye, and C. M. Lo, “Application of impact-echo method for rockbolt length detection,” *Constr. Build. Mater.*, vol. 316, p. 125904, Jan. 2022, doi: 10.1016/J.CONBUILDMAT.2021.125904.

[33] B. Sawicki, T. Piotrowski, and A. Garbacz, “Development of Impact-Echo Multitransducer Device for Automated Concrete Homogeneity Assessment,” *Materials 2021, Vol. 14, Page 2144*, vol. 14, no. 9, p. 2144, Apr. 2021, doi: 10.3390/MA14092144.

[34] H. N. Li, D. S. Li, and G. B. Song, “Recent applications of fiber optic sensors to health monitoring in civil engineering,” *Eng. Struct.*, vol. 26, no. 11, pp. 1647–1657, Sep. 2004, doi: 10.1016/J.ENGSTRUCT.2004.05.018.

[35] H. Wei, X. Zhao, D. Li, P. Zhang, and C. Sun, “Corrosion monitoring of rock bolt by using a low coherent fiber-optic interferometry,” *Opt. Laser Technol.*, vol. 67, 2015, doi: 10.1016/j.optlastec.2014.10.004.

[36] W. H. Glenn, W. W. Morey, and G. Meltz, “Formation of Bragg gratings in optical fibers by a transverse holographic method,” *Optics Letters, Vol. 14, Issue 15, pp. 823-825*, vol. 14, no. 15, pp. 823–825, Aug. 1989, doi: 10.1364/OL.14.000823.

[37] K. T. Lau, L. Yuan, L. M. Zhou, J. Wu, and C. H. Woo, “Strain monitoring in FRP laminates and concrete beams using FBG sensors,” *Compos. Struct.*, vol. 51, no. 1, pp. 9–20, Jan. 2001, doi: 10.1016/S0263-8223(00)00094-5.

[38] A. Barrias, J. R. Casas, and S. Villalba, “A Review of Distributed Optical Fiber Sensors for Civil Engineering Applications,” *Sensors 2016, Vol. 16, Page 748*, vol. 16, no. 5, p. 748, May 2016, doi: 10.3390/S16050748.